

NASA Reference Publication 1042

**Performance Evaluation Method
for Dissimilar Aircraft Designs**

Harold J. Walker

SEPTEMBER 1979

NASA

NASA Reference Publication 1042

Performance Evaluation Method for Dissimilar Aircraft Designs

Harold J. Walker
Dryden Flight Research Center
Edwards, California

NASA

National Aeronautics
and Space Administration

**Scientific and Technical
Information Branch**

1979

PERFORMANCE EVALUATION METHOD FOR DISSIMILAR AIRCRAFT DESIGNS

Harold J. Walker
Dryden Flight Research Center

INTRODUCTION

In design competition, the superiority of one aircraft concept over another depends largely on which design most effectively integrates the latest advances in aerodynamics, structures, propulsion, and controls. Often a number of potential, and sometimes unconventional, configurations must be evaluated before a final selection is made. It is particularly important that each of the competing designs be evaluated in terms of its relative improvement over the prior state of the art in each of the technologies, as well as its relative overall merit or performance.

A comparative performance evaluation from a disciplinary point of view requires the use of a nondimensional framework of parameters (such as aerodynamic coefficients, load factors, and thrust-to-weight ratios) to eliminate effects due to differences in scale. It has been customary to reduce all aerodynamic forces and moments to unit values based on the area of the wing planform, which is assumed to be the dominant lifting element. In some cases, however, this assumption may be inappropriate, particularly for configurations where substantial lift may arise from other components (such as the tail or canard surfaces, fuselage, strakes, and variable geometry features) or for blended configurations where the wing component itself is not clearly definable. As illustrated in figure 1, the configurations of interest may differ considerably in the arrangement of components and overall distribution of lift. Therefore, the selection of the wing or some other arbitrary surface as a reference area for achieving a common scale is likely to result in an incorrect assessment of the relative efficiency or performance of the designs being compared.

The major objective of this report is to develop a rationale for selecting the square of an aircraft's wingspan as the basis for comparative performance analysis. Parameters are developed for the comparison of basic aerodynamic performance

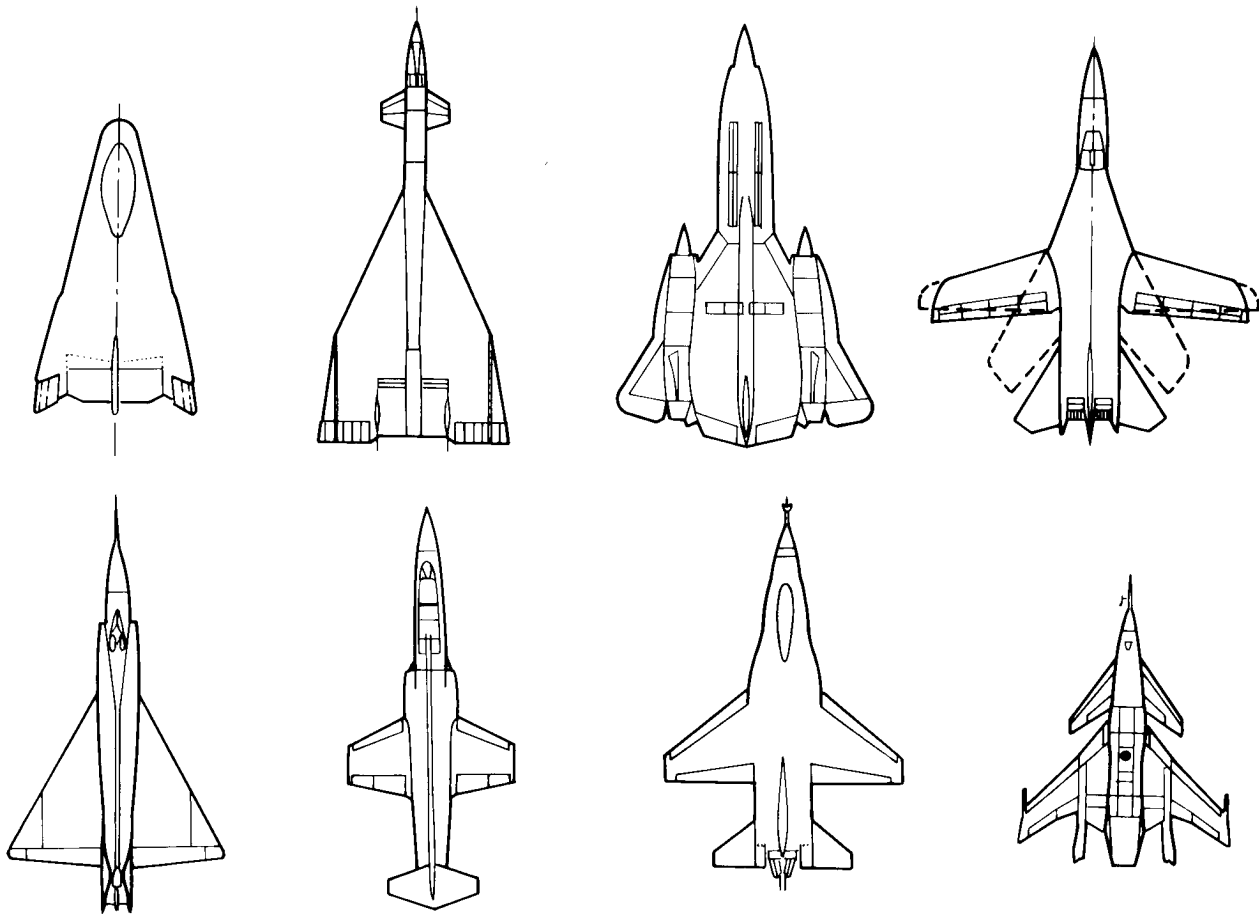


Figure 1. Typical configurations of interest in comparative performance analysis.

and are subsequently modified to determine the effects of aircraft loading and available thrust. A second objective of this report is to review briefly the performance trends of various categories of aircraft evaluated by NASA from the late 1940's to the present time. Both evaluation methods are applied to each category of aircraft and, to provide a measure of relative overall efficiency, a standard (or idealized) configuration is included for each category. Where possible, the data are taken from published flight test results to avoid uncertainties that could be attributed to major differences in test techniques and vehicle scale. In the development of the span-squared method, frequent use is made of the collective publications of Dr. Robert T. Jones (ref. 1).

It is the author's opinion that the square of the span is a more appropriate basis for performance comparison than the commonly used reference area. Therefore, in this report the results obtained by the span-squared method are presumed to be accurate, and the differences between the results of the span-squared and reference area methods are considered to represent inaccuracies in the reference area method.

SYMBOLS

Physical quantities are given in the International System of Units (SI) and parenthetically in U.S. Customary Units. Factors relating the two systems are given in reference 2.

A	aspect ratio, b^2/S_{ref} or b^2/S
b	aircraft span
C_D	drag coefficient, $\frac{D}{qS_{ref}}$ or $\frac{D}{qS}$
C_{D_i}	induced drag coefficient
C_{D_w}	wave drag coefficient at zero lift
C_F	average skin friction coefficient
C_L	lift coefficient, $\frac{L}{qS_{ref}}$ or $\frac{L}{qS}$
C_{L_α}	lift curve slope
c	wing local chord
c'	specific fuel consumption
D	drag
D_i	induced drag

D_o	zero-lift drag
D_w	wave drag at zero lift
$E'(m)$	complete elliptic integral of the second kind, modulus $\sqrt{1 - m^2}$
e	induced drag efficiency factor
$f(\cdot)$	function of (\cdot)
f_n	fuselage fineness ratio
h	altitude
K	$= \frac{S_w}{2S_p}$
k	induced drag factor
L	lift, nW
l	aircraft length
M	Mach number
m	$= \beta \cot \Lambda$
\bar{m}	mass
N	particular function of m (eq. (27))
n	load factor
Δp	upper surface pressure minus lower surface pressure
Q	aircraft volume
q	dynamic pressure, $1/2\rho V^2$
R	range

r	radius of an element of air mass (fig. 2(b))
S	wing area
S_B	fuselage maximum cross-sectional area
S_p	aircraft planform area
S_{ref}	reference area
S_w	aircraft wetted area
$S_{\overline{w}}$	area producing wave drag
T	thrust
t	time
t'	wing section thickness
V	aircraft velocity
v	vortex induced velocity (fig. 2(b))
W	aircraft weight
y	spanwise coordinate
α	angle of attack
β	$= \sqrt{M^2 - 1}$ or $\sqrt{1 - M^2}$
Γ	flow circulation
γ	flightpath angle
$\bar{\gamma}$	ratio of specific heat at constant pressure to specific heat at constant volume
ε	downwash angle
η	fraction of semispan, $2y/b$
θ, φ	angular position of an air mass element (fig. 2(b))

Λ	wing leading edge sweep angle
ρ	atmospheric density
ω	downwash velocity
$\bar{\omega}$	average downwash velocity

Subscripts:

<i>eff</i>	effective
<i>max</i>	maximum
<i>min</i>	minimum
<i>nor</i>	normal
<i>opt</i>	optimum
<i>0</i>	start of cruise
<i>1</i>	end of cruise
<i>1, 2</i>	vortex designation (fig. 2(b))

RATIONALE FOR SPAN-SQUARED METHOD

The basic principle underlying the flight of an aircraft (fig. 2(a)) is that circulatory flow occurs about the lifting surfaces such that the rate of the downward momentum imparted to the air is equal to the lift generated by the aircraft. In addition, the downwash in the wake produces a streamwise component of the resultant force, namely the induced or vortex drag, D_i . Thus,

$$L = \frac{d}{dt} \int \omega \, d\bar{m} = \int \omega \, d\left(\frac{d\bar{m}}{dt}\right) \quad (1a)$$

$$D_i = \int (\tan \varepsilon) \, dL \quad (1b)$$

where $d\bar{m}$ is an element of air mass, ω is the local downwash velocity, and ε is the local downwash angle. These expressions apply to the entire disturbed flow field in each transverse plane downstream from the wing. In more familiar form,

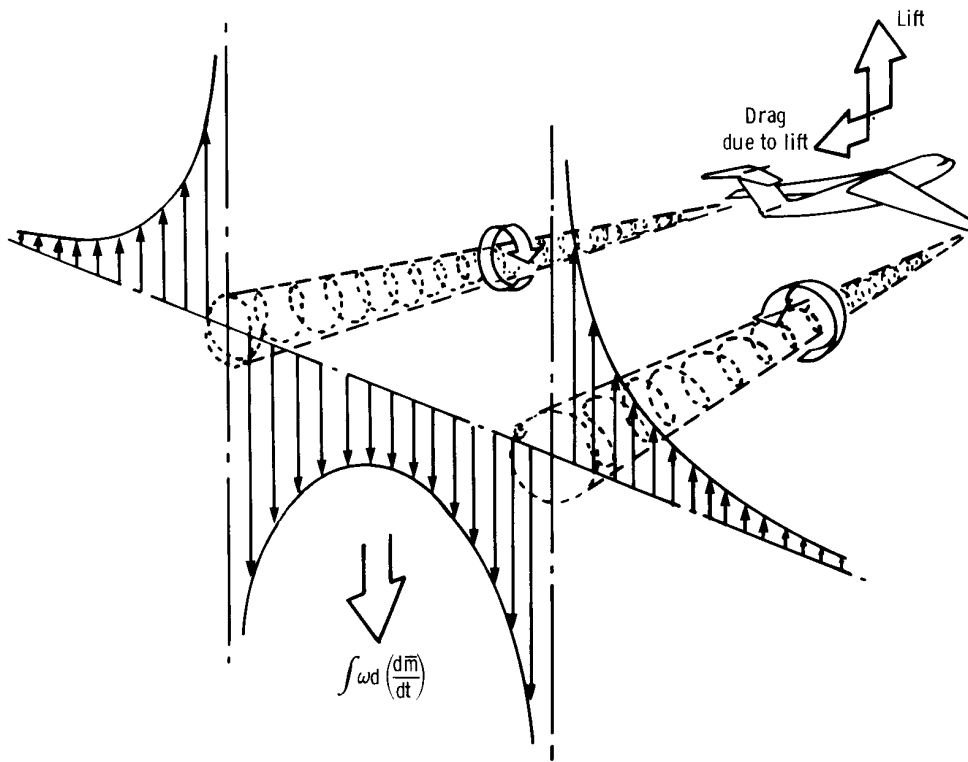
$$\frac{d\bar{m}}{dt} = \int \rho V r \, d\theta \, dr \quad (2a)$$

$$\tan \varepsilon \cong \omega/V \quad (2b)$$

$$L = \rho V^2 \iint (\omega/V) r \, d\theta \, dr \quad (2c)$$

$$D_i = \int (\omega/V) \, dL \quad (2d)$$

where $r \, d\theta \, dr$ is an element of the cross-sectional area in the downstream flow. At positions far downstream, the downwash pattern is independent of the chordwise distribution of circulation over the aircraft. This observation from reference 3 is the basis for the selection of the span squared as an aerodynamic scaling factor. The downwash, ω/V , imparted to the flow (and, hence, the lift and induced drag) is functionally related only to the span of the combined lifting elements (fig. 2(b)).



(a) Downwash pattern in transverse planes.

Figure 2. Schematic of basic principle of lifting vehicle.

Therefore, the integral of the flow field can be expressed only in terms of aircraft span. Thus, with reference to figure 2(b) and assuming the flow circulation ($\Gamma = r\omega$) to be constant, it can be shown that

$$\frac{\omega}{V} = \frac{2\Gamma}{bV} f\left(\frac{2r}{b}, \theta\right) \quad (3a)$$

which, upon substitution in equation (2c), leads to

$$L = \frac{1}{4} \rho b^2 V^2 \int_0^\infty \int_0^{2\pi} \left(\frac{2\Gamma}{bV}\right) f\left(\frac{2r}{b}, \theta\right) \left(\frac{2r}{b}\right) d\theta d\left(\frac{2r}{b}\right) \quad (3b)$$

In nondimensional form,

$$\frac{L}{qb^2} = \frac{1}{2} \int_0^\infty \int_0^{2\pi} \left(\frac{2\Gamma}{bV}\right) f\left(\frac{2r}{b}, \theta\right) \left(\frac{2r}{b}\right) d\theta d\left(\frac{2r}{b}\right) \quad (4a)$$

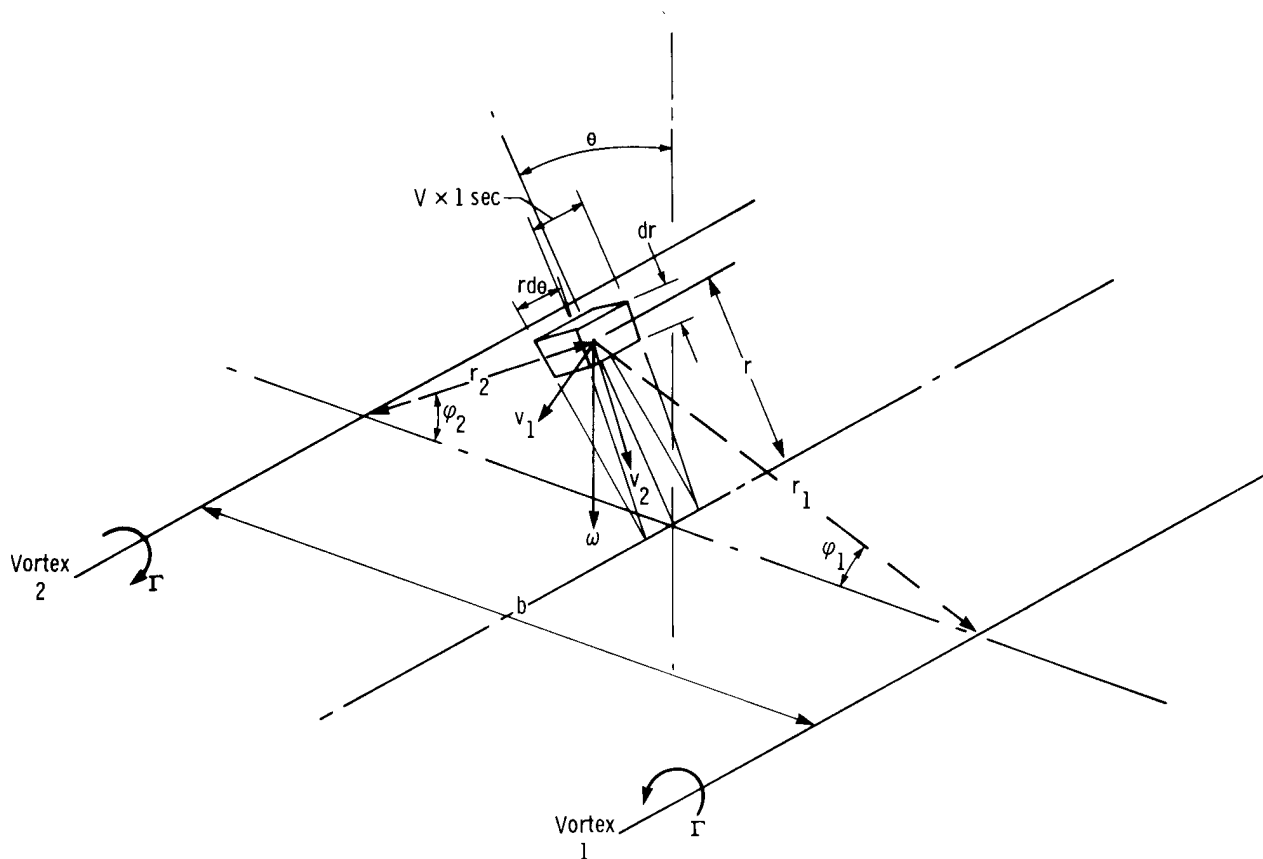
$$\frac{D_i}{qb^2} = \int (\omega/V) d\left(\frac{L}{qb^2}\right) \quad (4b)$$

It is reasonable to conclude from the above relationships that qb^2 is an appropriate basis for a common aerodynamic scale. Similar derivations are presented in the appendix for subsonic and supersonic flight conditions and for slender configurations. Since the mechanism of lift in a fluid medium is basically the same for all lifting elements, it is reasonable to expect that span-squared scaling should apply to all the aerodynamic coefficients (in addition to those for lift and drag) when various configurations are compared.

It is important to note that a reference area containing both chordwise and spanwise dimensions (rather than span squared) is an essential basis for studies involving structural load distributions and operational limitations such as flow separation, maximum lift, buffet onset, pitchup boundaries, and other phenomena that are dependent on angle of attack and, therefore, aspect ratio.

SPAN-SQUARED NOTATION

In this section, the principal performance relationships used in this study are outlined in span-squared notation. Relative performance is defined first in purely aerodynamic terms, then modifications are presented to show the effects of variations in aircraft loading and thrust-to-weight ratio.



$$\begin{aligned} \omega/V &= (v_1/V) \cos \varphi_1 + (v_2/V) \cos \varphi_2 \\ &= (\Gamma/r_1 V) \cos \varphi_1 + (\Gamma/r_2 V) \cos \varphi_2 \\ &= (2\Gamma/bV) f(2r/b, \theta) \end{aligned}$$

$$f(2r/b, \theta) = \frac{(2r/b) \sin \theta + 1}{(2r/b)^2 + 2(2r/b) \sin \theta + 1} - \frac{(2r/b) \sin \theta - 1}{(2r/b)^2 - 2(2r/b) \sin \theta + 1}$$

(b) Momentum transfer rate for fluid element.

Figure 2. Concluded.

Aerodynamic Efficiency

The drag polar at subsonic speeds is of the form

$$\frac{D}{qb^2} = \left(\frac{D_o}{qb^2} \right) + \left(\frac{1}{\pi e} \right) \left(\frac{L}{qb^2} \right)^2 \quad (5)$$

where, in most cases, the zero-lift drag, D_o , is due largely to skin friction. Aircraft with large base areas may also exhibit high afterbody pressure drag. The ratio of lift to drag (that is, aerodynamic efficiency) then is

$$\frac{L}{D} = \frac{L/qb^2}{D/qb^2 + (1/\pi e)(L/qb^2)^2} \quad (6a)$$

which has a maximum value of

$$\left(\frac{L}{D} \right)_{max} = \frac{1}{2\sqrt{(1/\pi e)(D_o/qb^2)}} \quad (6b)$$

which corresponds to

$$\left(\frac{L}{qb^2} \right)_{opt} = \sqrt{\pi e(D_o/qb^2)} \quad (6c)$$

As noted in the appendix, if the span loading is elliptical, e has an upper limit of 1 and full leading edge suction is obtained.

The above relationships also apply to slender configurations at supersonic speeds and all configurations near the speed of sound (see appendix).

At supersonic speeds, the efficiency factor e , as shown in the appendix, must account for wave drag as well as vortex drag. In general,

$$e = \frac{f(m)}{d(D/qb^2)/d(L/qb^2)^2} \quad (7a)$$

where m equals $\beta \cot \Lambda$, and $f(m)$ is a function of the shape of the lifting element. From the relationships developed in the appendix for a slender oblique wing aircraft at supersonic speeds,

$$f(m) = \frac{1}{\pi} \left(1 + \frac{m^2}{2} \right) \quad (7b)$$

For triangular configurations with subsonic leading edges ,

$$f(m) = \frac{1}{\pi} \left[2E(m) - \sqrt{1 - m^2} \right] \quad (7c)$$

For slender configurations , m approaches 0 and $f(m)$ is approximately $1/\pi$. At subsonic speeds, m equals 0 and $f(m)$ is simply $1/\pi$. With full leading edge suction, e has an upper limit of 1 .

Delta-shaped planforms with supersonic leading edges have lift and induced drag characteristics similar to those for a wing of infinite aspect ratio; namely (from ref. 1) ,

$$C_L = \frac{4}{\beta} \alpha \quad (8a)$$

$$C_{D_i} = C_L \alpha = \frac{4}{\beta} \alpha^2 \quad (8b)$$

In span-squared notation , the corresponding expressions are

$$\frac{L}{qb^2} = \frac{4}{\beta A} \alpha \quad (9a)$$

$$\frac{D_i}{qb^2} = \frac{4}{\beta A} \alpha^2 \quad (9b)$$

which yield

$$e = \frac{\beta A / 4}{d(D/qb^2)/d(L/qb^2)^2} \quad (10)$$

The zero-lift drag at supersonic speeds is expressed in terms of wave drag due to thickness as well as skin friction and afterbody pressure drag .

Loading Effects

The effect of aircraft weight on performance is obtained by expressing L/qb^2 in the form

$$\frac{L}{qb^2} = (L/W) (W/qb^2) \quad (11)$$

where L/W is the load factor and W/qb^2 represents the span loading in nondimensional form. The lift-to-drag ratio then becomes

$$\frac{L}{D} = \frac{(L/W)(W/qb^2)}{(D_o/qb^2) + (k/e)(L/W)^2(W/qb^2)^2} \quad (12)$$

where k equals $1/\pi$ for subsonic speeds and $f(m)$ for supersonic speeds.

When several aircraft are compared at a common span loading and load factor, aerodynamic efficiency determines which aircraft has the best performance.

Solving equation (12) for load factor gives

$$\frac{L}{W} = \frac{1}{2(L/D)(k/e)(W/qb^2)} \left[1 \pm \sqrt{1 - 4 \frac{k}{e} \left(\frac{L}{D}\right)^2 (D_o/qb^2)} \right] \quad (13)$$

This expression shows that, for a given lift-to-drag ratio, the aircraft with the lowest span loading (W/qb^2) is the most maneuverable.

Thrust Effects

Under steady-state conditions, the required ratio of thrust to weight may be expressed in the form

$$\frac{T}{W} = \frac{L/W}{L/D} \quad (14)$$

On a plot of L/D as a function of L/W , constant levels of T/W would appear as a series of lines radiating from the origin.

The highest load factor in horizontal flight at a given altitude is reached when the available thrust-to-weight ratio is at a maximum. Thus, substituting

$$\frac{L}{D} = \frac{L/W}{D/W} = \frac{L/W}{T_{max}/W} \quad (15)$$

in equation (12) and solving for L/W gives

$$\left(\frac{L}{W}\right)_{max} = \frac{1}{W/qb^2} \sqrt{\frac{e}{k} \left(\frac{T_{max}}{W} \frac{W}{qb^2} - \frac{D_o}{qb^2} \right)} \quad (16)$$

The maximum climb angle, γ_{max} , is obtained from the relationships

$$\sin \gamma = \frac{T_{max} - D}{W} = \frac{T_{max}}{W} - \frac{D_o/qb^2}{W/qb^2} - \frac{k}{e} \left(\frac{L}{W}\right)^2 \quad (17a)$$

$$\cos \gamma = L/W \quad (17b)$$

Solving for $\sin \gamma$ results in

$$\sin \gamma = \frac{e}{2k(W/qb^2)} - \sqrt{\left(\frac{e}{2k(W/qb^2)}\right)^2 - \frac{e}{k(W/qb^2)} \left(\frac{T_{max}}{W} - \frac{D_o/qb^2}{W/qb^2}\right) + 1} \quad (18)$$

An approximate solution is obtained by dropping the $\sin^2 \gamma$ term after substituting $\cos^2 \gamma$ for $(L/W)^2$ in equation (17a); namely,

$$\gamma = \sin^{-1} \left\{ \frac{1}{W/qb^2} \left[\frac{T_{max}}{W} \frac{W}{qb^2} - \frac{D_o}{qb^2} - \frac{k}{e} \left(\frac{W}{qb^2}\right)^2 \right] \right\} \quad (19)$$

In using the above equations, the efficiency factor, e , may vary with L/W , in which case a trial and error procedure will be required.

For zero thrust, the steady-state descent rate is simply

$$\gamma = -\sin^{-1} \left(\frac{1}{L/D} \right) \quad (20)$$

Range

The range of an aircraft is often an important consideration in performance comparisons. For a jet aircraft operating at a maximum lift-to-drag ratio and a given Mach number, the range is given by

$$dR_{max} = -\frac{V}{c'} \left(\frac{L}{D}\right)_{max} \frac{dW}{W} \quad (21)$$

where c' is the specific fuel consumption, which is assumed to be constant. Velocity then varies such that

$$W/qb^2 = (L/qb^2)_{opt} \quad (22a)$$

or

$$V = \sqrt{\frac{2}{\rho} \frac{W/b^2}{(L/qb^2)_{opt}}} \quad (22b)$$

The initial velocity is given by

$$V_0 = \sqrt{\frac{2}{\rho} \frac{W_0/b^2}{(L/qb^2)_{opt}}} \quad (23)$$

where W_0 is the initial weight. Above the tropopause, the velocity is constant; equation (21) may then be written as

$$\begin{aligned} dR &= - \frac{(L/D)_{max}}{c'} \sqrt{\frac{2}{\rho} \frac{W/b^2}{(L/qb^2)_{opt}}} \frac{dW}{W} \\ &= - \frac{(L/D)_{max}}{c'b} \sqrt{\frac{2}{\rho(L/qb^2)_{opt}}} \frac{dW}{\sqrt{W}} \end{aligned} \quad (24)$$

where all terms except W are constant. Integration between the limits W_0 and W_1 gives

$$R_{max} = \frac{(L/D)_{max}}{c'} \sqrt{\frac{2}{\rho(L/qb^2)_{opt}}} \frac{2\sqrt{W_0}}{b} \left(1 - \sqrt{\frac{W_1}{W_0}}\right) \quad (25)$$

Because W_0/qb^2 can be substituted for $(L/qb^2)_{opt}$, equation (25) reduces to

$$R = \frac{2}{c'} \left(\frac{L}{D}\right)_{max} V_0 \left(1 - \sqrt{\frac{W_1}{W_0}}\right) \quad (26)$$

STANDARD CONFIGURATION

A standard, or idealized, configuration is useful in providing an upper limit for assessing the overall efficiency or merit of a series of competitive designs and for providing a relative measure of additional gains that might be realized at each flight condition through improved span load distribution and reduced zero-lift drag. Since aircraft designed for different missions vary significantly in size, shape, propulsion, structural load limits, and other characteristics, the standard configuration would be expected to vary from one category to another. In the present study, it is also assumed that the standard configuration for a particular category of aircraft varies from one flight regime to another.

For subsonic and low supersonic Mach numbers (less than 1.5), the standard configuration is considered to be an oblique wing aircraft (fig. 3, from ref. 1) having elliptic span loading and thickness distribution, and a drag polar of the form given in the appendix. The area distribution is assumed to be the equivalent of that of an optimum supercritical body of revolution for transonic speeds (ref. 1). Overall dimensions, wetted areas, and surface loadings are chosen so as to conform with the existing state of the art for each category of aircraft.

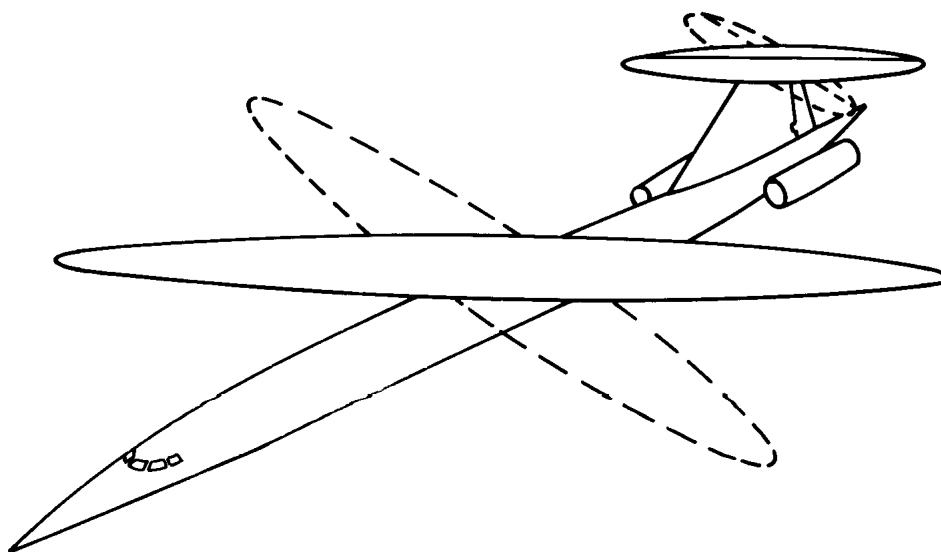


Figure 3. Oblique wing standard aircraft (ref. 1). $M < 1.50$.

For Mach numbers greater than 1.5, the standard configuration is assumed to be an arrow-wing aircraft (fig. 4) with subsonic leading edges and trailing edges parallel to the Mach lines. From reference 1, the lift and drag due to lift for this configuration are

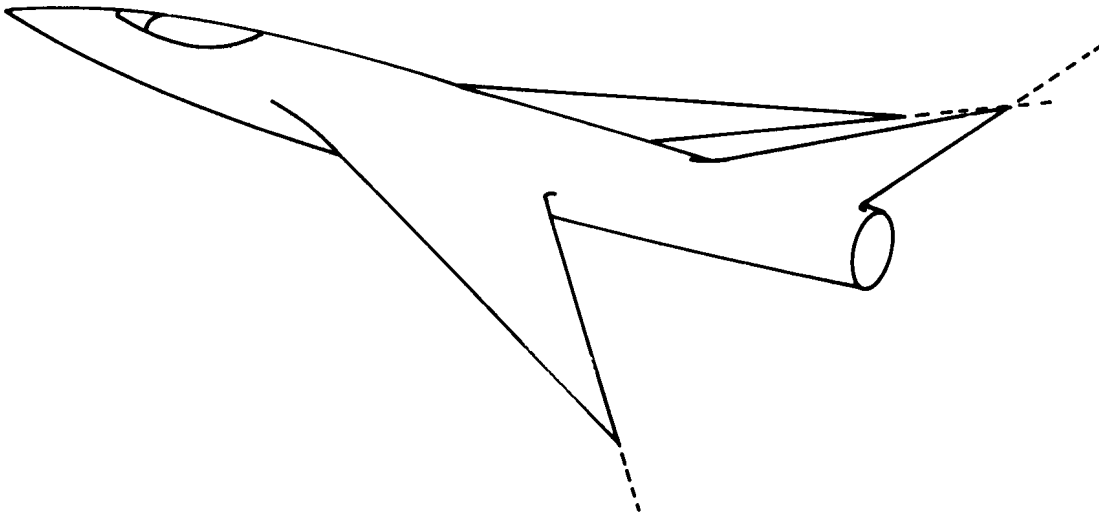


Figure 4. Arrow-wing standard configuration. $M > 1.50$; dashed lines indicate Mach lines.

$$C_L = \frac{4m\alpha}{\beta[E'(m)]\sqrt{1-m^2}} \left[\frac{\cos^{-1}(-m)}{1+m} + m\sqrt{\frac{1-m}{1+m}} \right] \quad (27a)$$

$$C_{D_i} = C_L^2 \left(\frac{1}{C_{L\alpha}} - \frac{\beta N^2}{4\pi m} \sqrt{\frac{1+m}{1-m}} \right) \quad (27b)$$

where

$$N = \frac{(\pi/2)\sqrt{1-m^2}}{\frac{\cos^{-1}(-m)}{1+m} + m\sqrt{\frac{1-m}{1+m}}} \quad (27c)$$

$E'(m)$ is the complete elliptic integral of the second kind of the modulus $\sqrt{1-m^2}$, and the aspect ratio is fixed by the condition

$$A = \frac{4m}{\beta(1-m)} \quad (28)$$

In span-squared notation,

$$\frac{L}{qb^2} = \frac{\pi\alpha(1-m)}{2N[E'(m)]} \quad (29a)$$

$$\frac{D_i}{qb^2} = \left(\frac{L}{qb^2}\right)^2 \left\{ \frac{2N}{\pi(1-m)} \left[E'(m) - \frac{N}{2} \sqrt{\frac{1+m}{1-m}} \right] \right\} \quad (29b)$$

When all edges are supersonic, the lift and drag due to lift can be expressed as

$$\frac{L}{qb^2} = \frac{\alpha^2}{A} \left\{ \frac{\bar{\gamma} + 1}{2} + \sqrt{\left(\frac{\bar{\gamma} + 1}{2}\right)^2 + \left(\frac{2}{\beta\alpha}\right)^2} - \frac{2}{\bar{\gamma}\beta^2\alpha^2} \left[\left(1 - \frac{\bar{\gamma} - 1}{2} \beta\alpha\right)^{\frac{2\bar{\gamma}}{\bar{\gamma} - 1}} - 1 \right] \right\} \quad (30a)$$

$$\frac{D_i}{qb^2} = \alpha \frac{L}{qb^2} \quad (30b)$$

These expressions, from reference 5, are derived from the unified supersonic-hypersonic theory presented in reference 6.

PERFORMANCE COMPARISONS

In this section, typical performance comparisons are presented for several categories of aircraft using both the reference area and the span-squared scaling methods. To insure the applicability of the span-squared method, performance comparisons are made for various aircraft and flight conditions for each of the following five categories: NACA research aircraft ($M = 0.90$), century-series fighter aircraft ($M = 1.15$), F-111A and F-111 transonic aircraft technology (TACT) configurations ($M = 0.90$), lifting-body-series aircraft ($M = 0.60$), and supersonic aircraft ($M = 2.00$). A standard configuration similar to those illustrated in figures 3 and 4 is also included in each category. The lift and drag coefficients for these aircraft were obtained mainly from published flight test results; the span-squared coordinates were obtained simply by dividing the coefficients by aspect ratio. These data illustrate the inaccuracies that may occur when conventional reference areas are used as the basis for performance comparisons. Although the differences in the performance capabilities of the various aircraft are of interest, the principal emphasis in this report is on the differences in the results for the two methods of scaling.

NACA Research Aircraft

In general, the NACA research aircraft were designed to achieve a limited number of specific goals in an unknown environment. As illustrated in figure 5, these aircraft vary considerably in planform. In particular, the proportion of the planform area that was used as the reference area during the development of each aircraft varies noticeably among the aircraft in the group. The X-1E, D-558-II, and X-15 aircraft were rocket powered, whereas the XF-92A, X-3, and X-5 aircraft were jet powered. The X-1E and D-558-II aircraft could be flown at supersonic speeds and the X-15 aircraft at hypersonic speeds. The only common Mach number that allowed a satisfactory performance comparison of the group was 0.90. An altitude of 10,700 meters (35,000 ft) was assumed. A number of parameters of interest in comparing these aircraft are listed in table 1; further details are given in references 7 to 13.

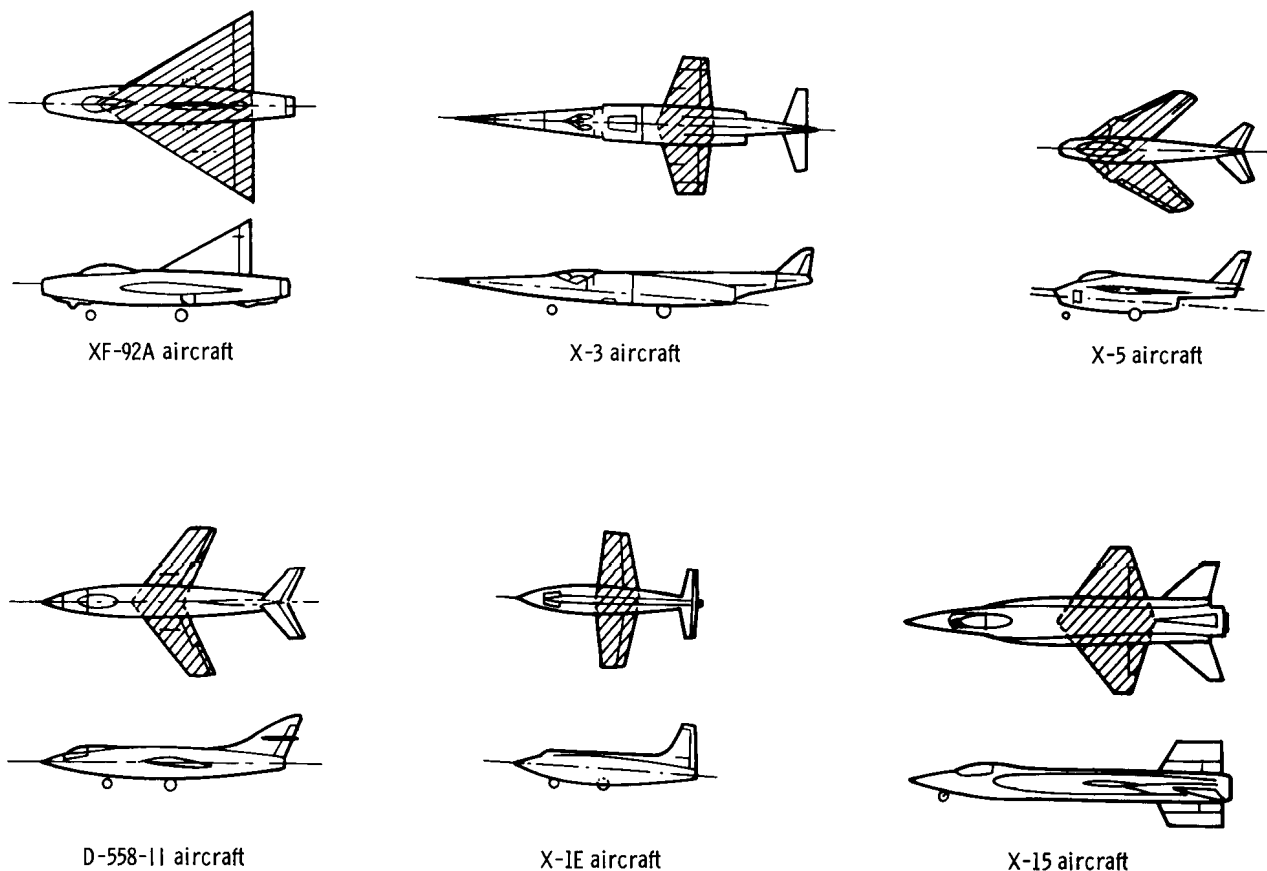


Figure 5. NACA research aircraft with reference areas shaded.

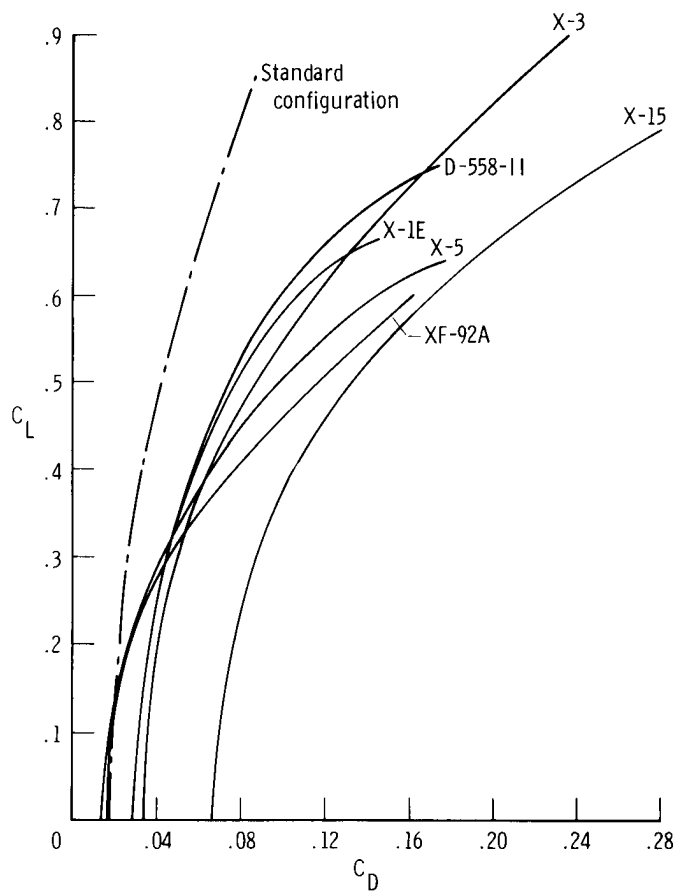
TABLE 1. CHARACTERISTICS OF NACA RESEARCH AIRCRAFT

[M 0.90; h 10,700 m (35,000 ft); q 13.50 kN/m² (283 lb/ft²)]

	Configuration						
	X 1E	XF 92A	D-558-II	X 3	X 5	X-15	Standard
b, m (ft)	6.95 (22.8)	9.54 (31.3)	7.62 (25.0)	6.92 (22.7)	6.10 (20.0)	6.71 (22.0)	7.89 (25.9)
S, m ² (ft ²)	12.1 (130.0)	39.5 (425.0)	16.3 (175.0)	15.5 (166.5)	17.1 (184.3)	18.6 (200.0)	18.6 (200.0)
S _w , m ² (ft ²)	57.9 (623)	131.9 (1420)	75.2 (809)	101.5 (1093)	70.4 (758)	106.6 (1147)	83.6 (900)
S _p , m ² (ft ²)	20.6 (222)	45.0 (484)	31.4 (338)	33.8 (364)	24.2 (261)	39.3 (423)	29.7 (320)
K	1.40	1.47	1.20	1.50	1.45	1.35	1.40
W _{min} , kN (lb)	36.1 (8120)	52.5 (11,800)	41.9 (9420)	72.6 (16,300)	34.9 (7850)	65.4 (14,700)	44.48 (10,000)
W _{max} , kN (lb)	70.9 (15,950)	69.2 (15,560)	70.2 (15,800)	98.3 (22,100)	44.3 (9960)	146.8 (33,000)	44.48 (10,000)
W _{nor} , kN (lb)	46.60 (10,470)	57.55 (12,940)	50.40 (11,330)	80.30 (18,050)	37.70 (8480)	106.00 (23,850)	44.48 (10,000)
W _{nor} /S, kN/m ² (lb/ft ²)	3.830 (80)	1.435 (30)	3.110 (65)	5.170 (108)	2.200 (46)	5.700 (119)	2.395 (50)
qb ² , kN (lb)	654.0 (147,000)	1233.0 (277,300)	787.0 (176,900)	648.5 (145,800)	503.5 (113,200)	609.4 (137,000)	849.6 (191,000)
W _{nor} /qb ²	0.0712	0.0466	0.0639	0.1236	0.0749	0.1740	0.0527
D _o /qb ²	0.00626	0.00584	0.00784	0.01100	0.00833	0.02640	0.00506
S _w /b ²	1.20	1.45	1.30	2.12	1.90	2.37	1.35
T _{max} , kN (lb)	26.70 (6000)	9.56 (2150)	34.80 (7820)	15.90 (3570)	7.36 (1655)	253.50 (57,000)	44.48 (10,000)
T _{max} /W _{nor}	0.573	0.166	0.690	0.198	0.195	2.390	0.573

The standard configuration for this category is assumed to be an oblique wing aircraft with optimum wing-fuselage blending and an elliptical planform with an aspect ratio of 4.25 in the unskewed position. A skew angle of 27° was chosen to obtain a Mach number of 0.80 normal to the lateral axis of the wing when the aircraft is operating at a Mach number of 0.90. With the wing in the skewed position, the aspect ratio is reduced to 3.35. The wing planform was expected to be compatible with the structural technology used in the design of the NACA research aircraft and was determined principally from assumed average thickness-to-chord and thickness-to-semispan ratios of 0.05 and 0.03, respectively. Skin friction and wave drag for the wing and fuselage were estimated by the methods described in reference 14. The wetted area was assumed to be proportional to the total planform area (multiplied by 2). A proportionality factor, K, of 1.4 was considered to be representative of the aircraft in the group. The fuselage was assumed to have a maximum diameter equal to 15 percent of the wingspan and a fineness ratio of 12. The vehicle size was determined from an assumed wing surface loading of 240 newtons per square meter (50 lb/ft²) and an assumed vehicle normal weight (with 30-percent fuel) of 44.48 kilonewtons (10,000 lb). The characteristics of interest are summarized in table 1.

The drag polars for this series based on reference area and span-squared coordinates are shown in figures 6(a) and 6(b), respectively. Near zero lift, the XF-92A aircraft shows the lowest drag of the group in both systems; however, the X-1E aircraft shifts to a much lower level and the X-5 aircraft to a relatively high level when converted to the span-squared system. At high lift, the order of the polars is noticeably different in the span-squared system, with the D-558-II and X-1E aircraft showing relatively high levels of drag and the X-5 aircraft showing the lowest level. In either system, the drag values for the X-15 aircraft are much greater than those for the earlier aircraft due to the large base of the X-15 aircraft's vertical tail. All the polars for the NACA research aircraft deviate substantially from the polar for the standard configuration because of the unfavorable span loadings of the aircraft.

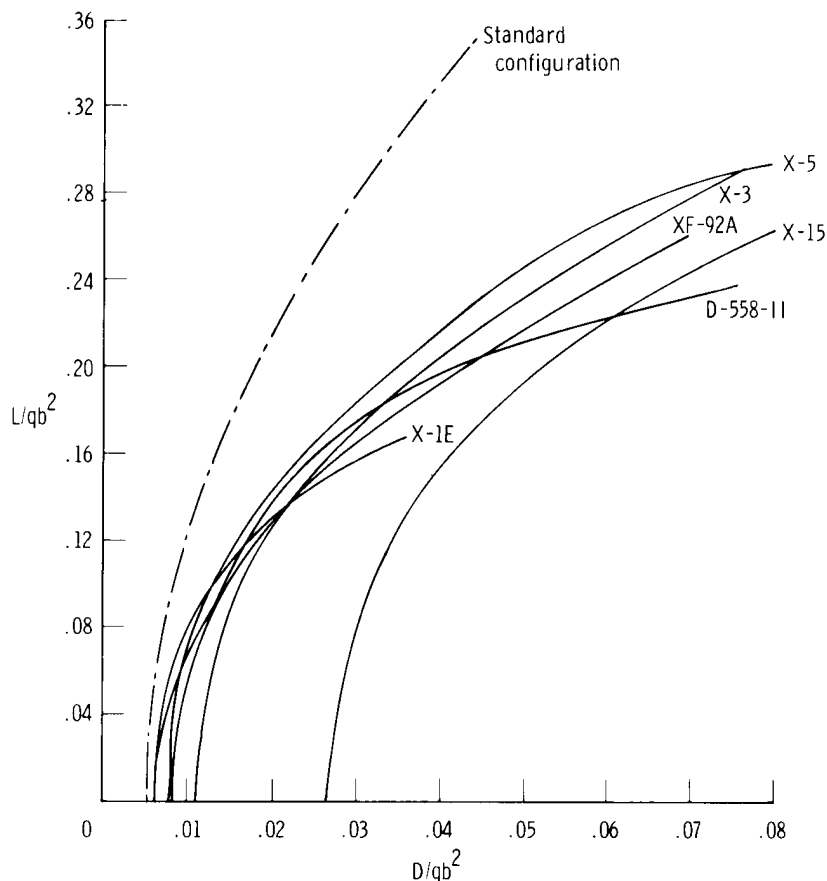


(a) C_L versus C_D .

Figure 6. Comparison of drag polars for NACA research aircraft. $M = 0.90$.

A comparison of lift-to-drag ratios in the two scaling systems is given in figure 7. As in the drag polars in figure 6, notably different trends are exhibited, particularly in the high-lift range. Although the relative levels for the XF-92A, X-3, and X-15 aircraft are roughly the same in both systems, the D-558-II and X-1E aircraft assume much lower levels in the span-squared notation whereas the X-5 aircraft rises to the highest level. These differences are consistent with the trends of the drag polars, and together the two comparisons illustrate the ambiguity that may arise when aerodynamic efficiency is judged on the basis of reference area rather than span-squared coefficients. All the aircraft are considerably lower in efficiency than the standard configuration.

As shown in figure 8, efficiency factor, e , as a function of lift is less sensitive to scaling method than the drag polars and lift-to-drag ratios. Only the D-558-II and X-1E aircraft vary noticeably between scaling methods. All the aircraft except the X-1E aircraft show large losses in efficiency in the upper lift range due mainly to shock-induced flow separation.

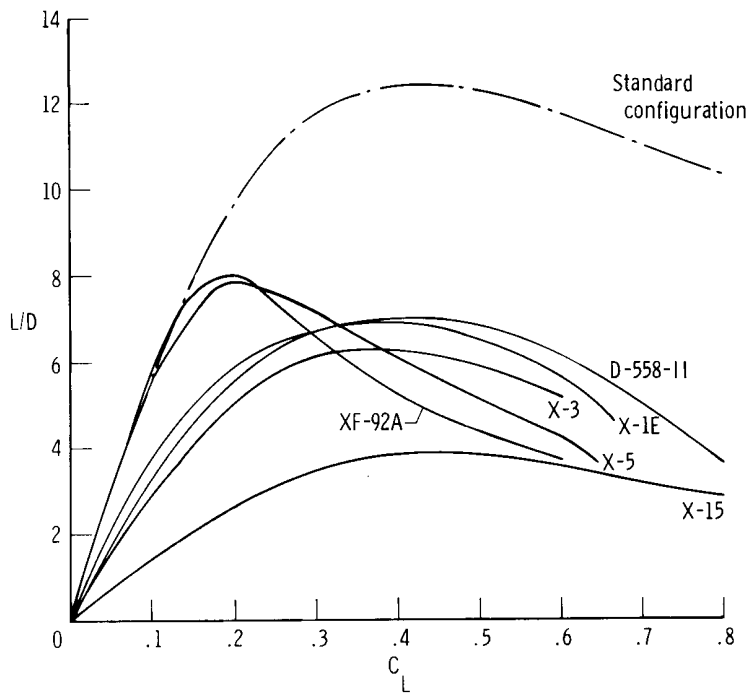
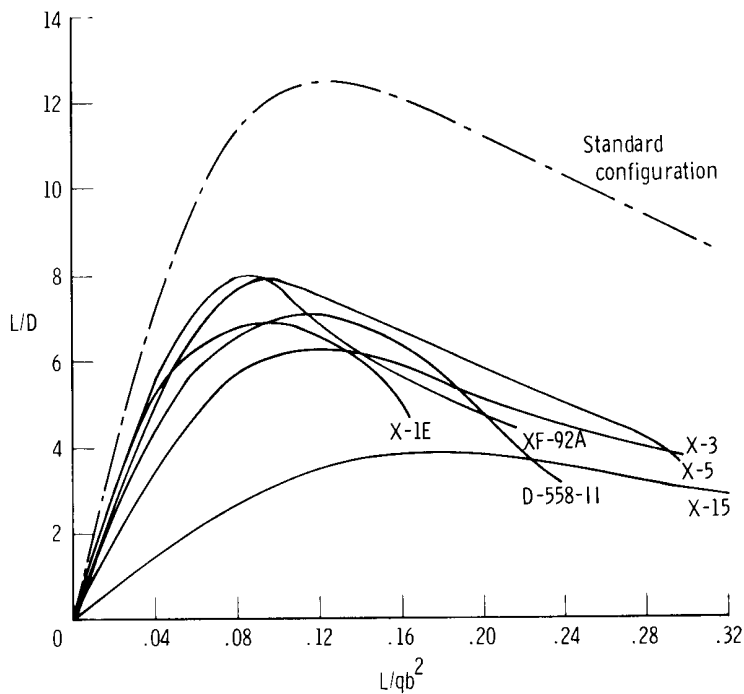


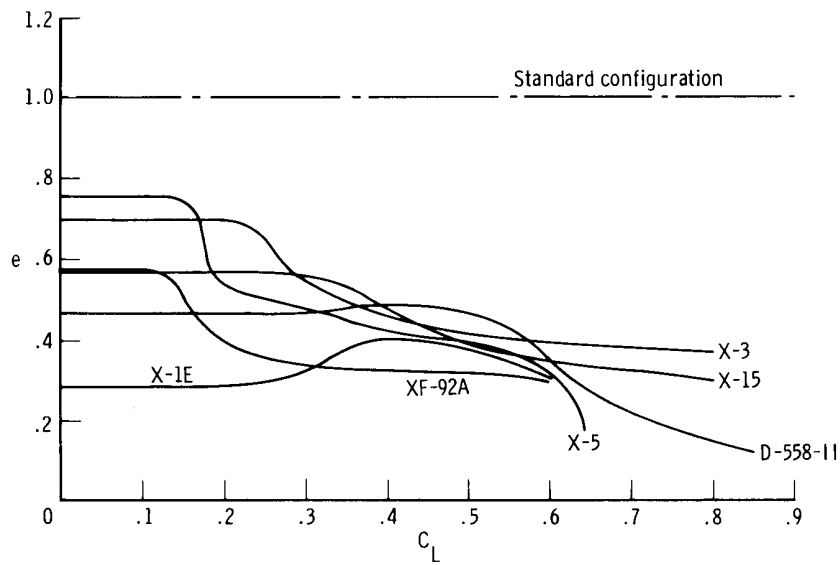
(b) L/qb^2 versus D/qb^2 .

Figure 6. Concluded.

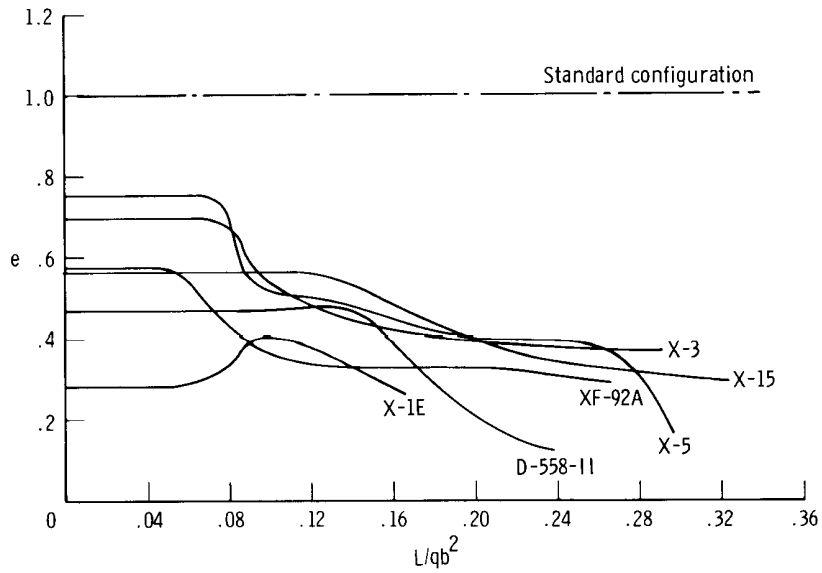
Figure 9 shows the variations of load factor with lift (that is, maneuverability) as expressed in the two scaling systems. The normal aircraft weights given in table 1 are assumed. Considerable shifting between the two systems is noted for the D-558-II, X-1E, and X-5 aircraft. The maneuvering limits due to available thrust at an altitude of 10,700 meters (35,000 ft) are indicated in figure 9(b), which shows the maneuverability of the jet-powered aircraft (the XF-92A, X-5, and X-3 aircraft) to be marginal.

A more complete representation of the performance characteristics of the aircraft in this series is given in figure 10, which shows the relationship between load factor, lift-to-drag ratio, and thrust-to-weight ratio. The delta-wing XF-92A aircraft has the highest efficiency at high load factors but insufficient thrust to reach those levels. The X-1E, X-3, and X-5 aircraft have the best performance at low load factors, but all the aircraft fall considerably short of the standard configuration in the normal operating range. It is important to note that the reason the XF-92A aircraft has the highest efficiency is not because it has the highest lift-to-drag ratio (fig. 7(b)), but rather because it has a low span loading, W/qb^2 (table 1). Conversely, the maneuver performance of the X-3 aircraft is degraded by its high span loading.

(a) L/D versus C_L .(b) L/D versus L/qb^2 .Figure 7. Comparison of aerodynamic efficiencies of NACA research aircraft. $M = 0.90$.



(a) e versus C_L .



(b) e versus L/qb^2 .

Figure 8. Comparison of efficiency factors for NACA research aircraft. $M = 0.90$.

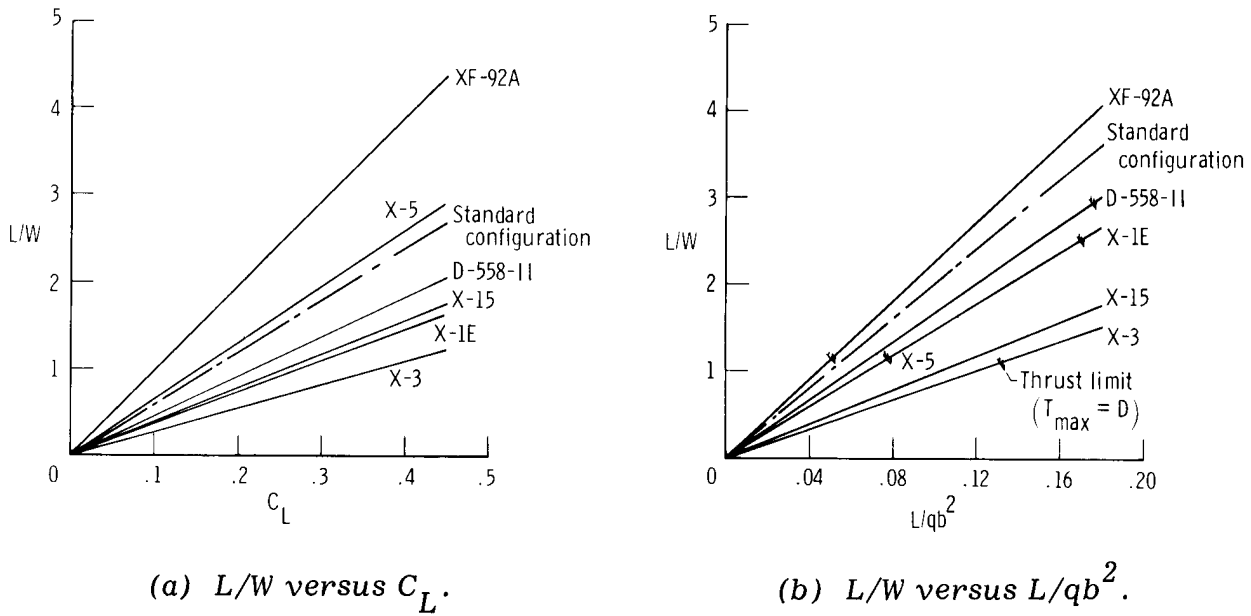


Figure 9. Maneuverability comparison of NACA research aircraft. $M = 0.90$; $h = 10,700$ meters (35,000 ft); normal weights (table 1).

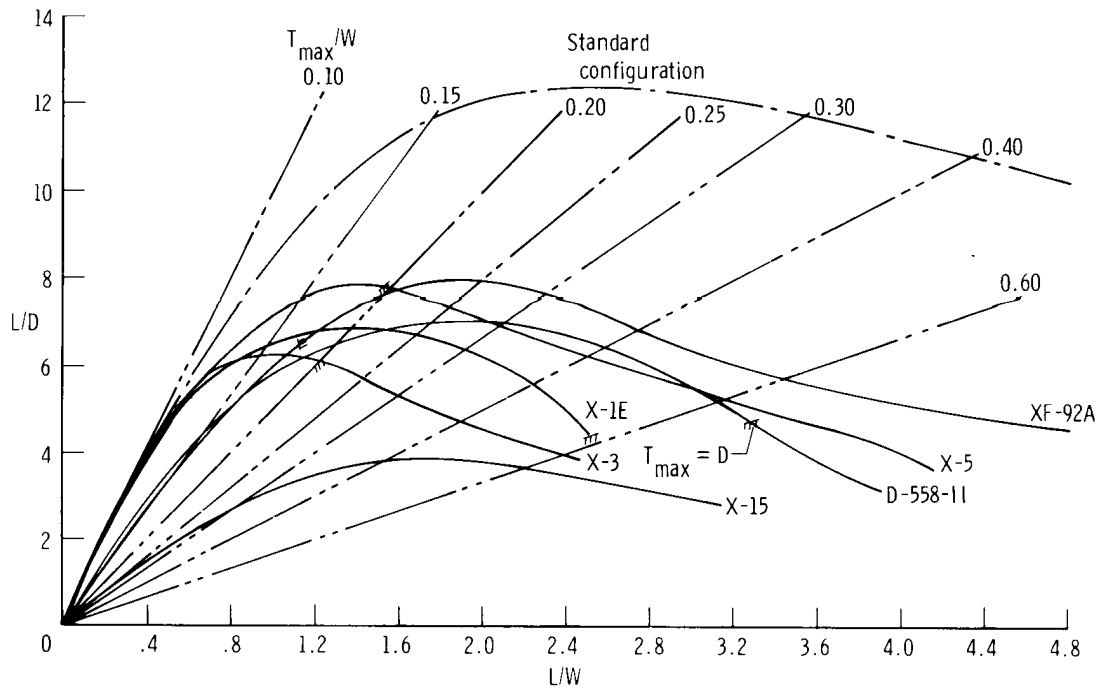
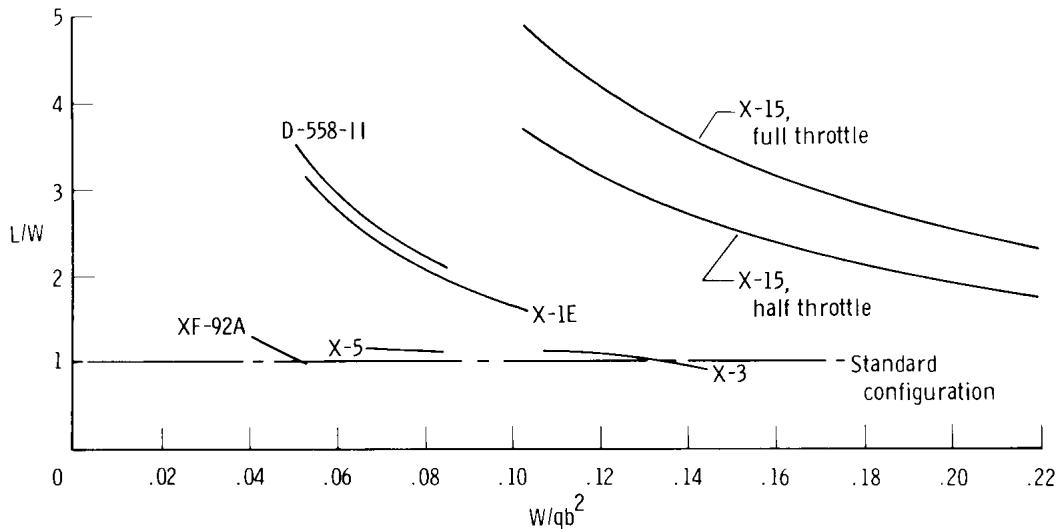


Figure 10. Performance comparison of NACA research aircraft. $M = 0.90$; $h = 10,700$ meters (35,000 ft); normal weights (table 1).

The effect of span loading on maneuverability is shown in figure 11(a) for conditions corresponding to maximum available thrust (fig. 10). It is quite evident that the three jet-powered aircraft had little maneuver margin at Mach 0.90 and an altitude of 10,700 meters (35,000 ft) as compared with the rocket-powered aircraft, which had much higher thrust-to-weight ratios. Similar trends are shown in figure 11(b) for maximum climb angle. The minimum glide slopes shown in this figure reflect the range of maximum lift-to-drag ratios for this series.



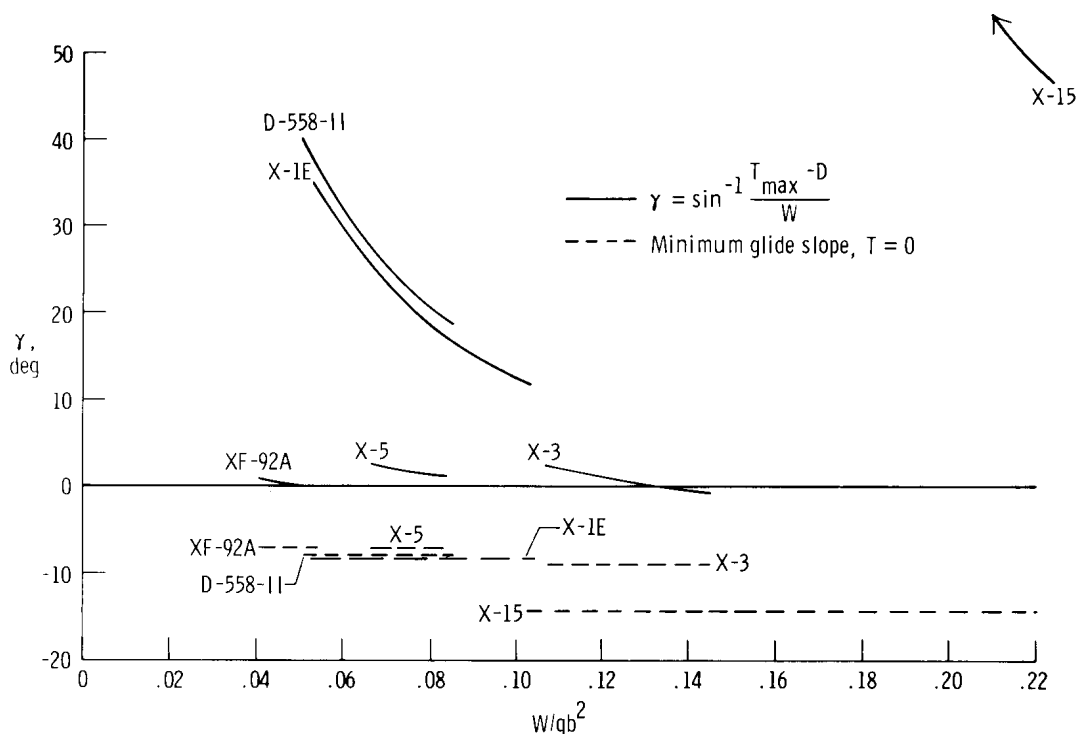
(a) Load factor.

Figure 11. Effect of span loading on performance of NACA research aircraft. $M = 0.90$; $h = 10,700$ meters (35,000 ft); $T_{max} = D$.

Century-Series Fighter Aircraft

The century series of fighter aircraft consists of the six aircraft illustrated in figure 12. The characteristics of these aircraft, which have a wide range of design features, are listed in table 2 for a low supersonic speed. The F-111 TACT airplane, although not an early member of the century series, is included to broaden the comparative range of planforms and reference areas. The YF-102 and F-102A airplanes have cambered delta wings and are nearly identical except that the latter is an area-rule (Whitcomb) design and is equipped with an engine of higher thrust. The F-104 airplane has a straight tapered wing, the F-100 and F-111 TACT airplanes have swept wings (with maximum sweep angles of 45° and 58° , respectively), and the F-4D airplane features a delta-like wing with rounded tips. These aircraft are compared at a Mach number of 1.15 and an altitude of 10,700 meters (35,000 ft). The data were obtained from references 15 to 19.

The standard configuration for this series is assumed to be identical to the elliptical oblique wing design chosen for the NACA research aircraft series. The wing, however, is skewed to an angle of 45° so that the Mach number component



(b) Climb angle.

Figure 11. Concluded.

normal to the wing lateral axis is held at 0.80. The wing aspect ratio is then reduced to 3.00 and the span to 7.47 meters (24.5 ft). As with the research aircraft, the zero-lift drag (skin friction and wave drag) was determined by the methods of reference 14, and the span loading was assumed to be elliptical ($e = 1$). The principal characteristics of this configuration are given in table 2.

The drag polars for these aircraft in the reference area and span-squared systems are shown in figures 13(a) and 13(b), respectively. Several striking changes in the order of the polars are apparent when the two systems are compared. Near zero lift, the drag of the F-100 airplane is reduced from an intermediate level in the reference area system to the lowest level in the span-squared system. The drag of the F-111 TACT airplane, on the other hand, is increased to the highest level of the group near zero lift. The F-100 airplane also shows a relatively high level of drag with increasing lift. Otherwise, the order of the drag polars is fairly consistent. All the drag polars except that of the F-111 TACT airplane in the span-squared system (fig. 13(b)) deviate considerably from the elliptical form of the polar for the standard configuration.

The lift-to-drag ratios in figure 14 show that the displacements of the maximum levels for the F-100 and F-111 TACT airplanes are in accord with the differences noted in the drag polars between the two scaling systems. The ratio is highest for the F-100 airplane and lowest for the F-104 airplane. The three delta-wing aircraft have similar reference areas and, therefore, a fixed relationship in both scaling systems. With an improved area distribution, the F-102A airplane, as expected,

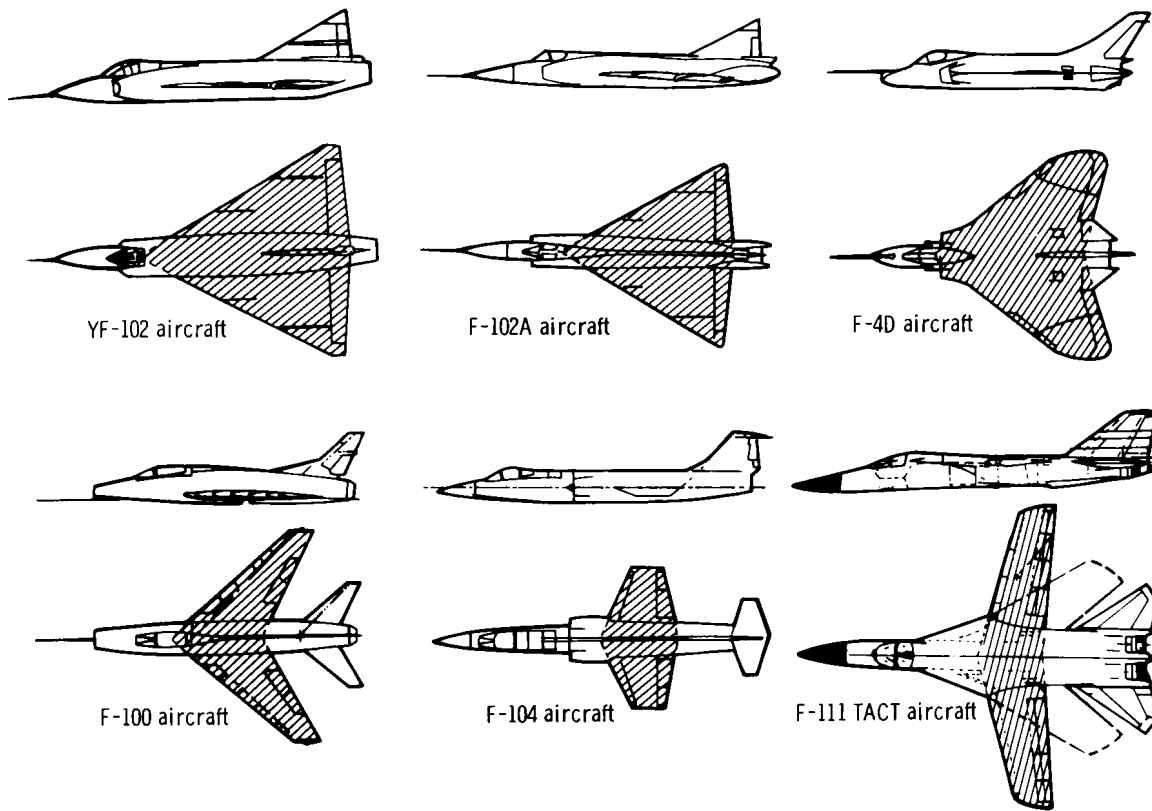
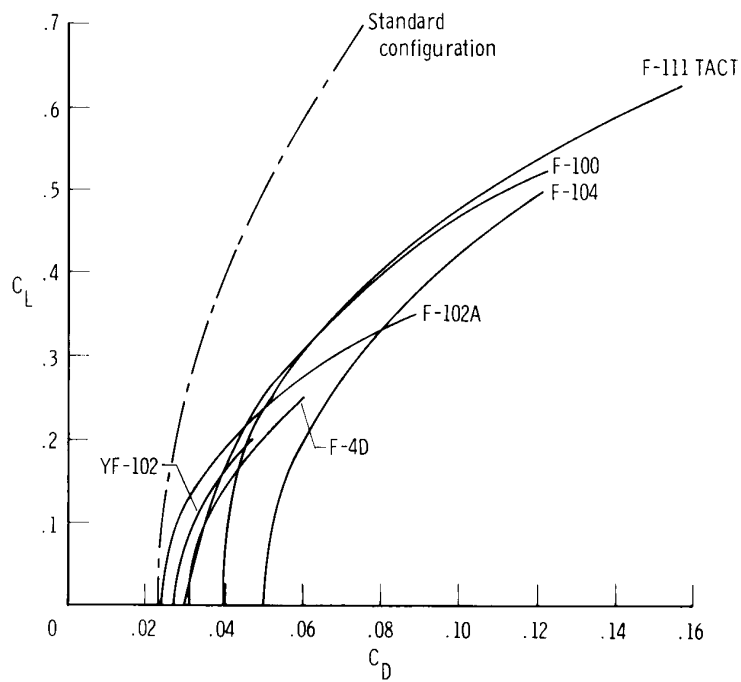
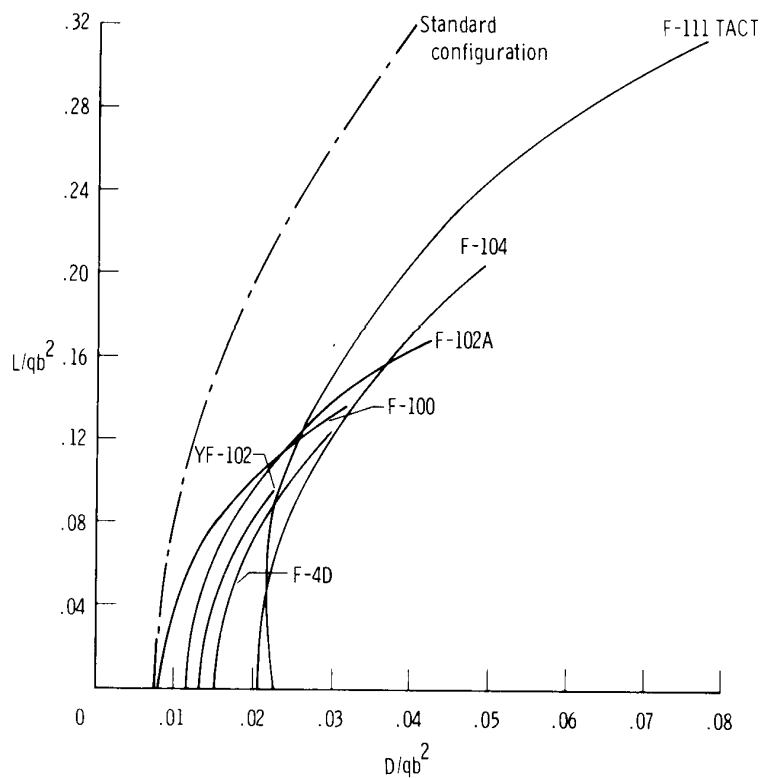


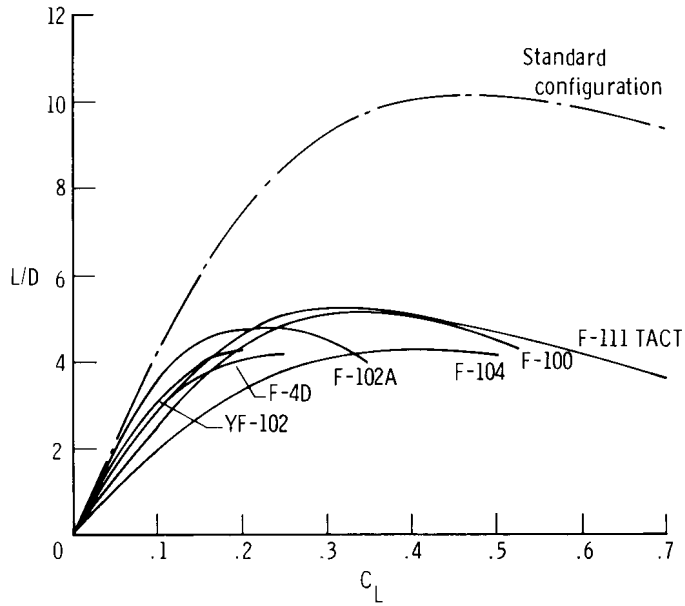
Figure 12. Century-series fighter aircraft with reference areas shaded.

TABLE 2. --CHARACTERISTICS OF CENTURY-SERIES FIGHTER AIRCRAFT

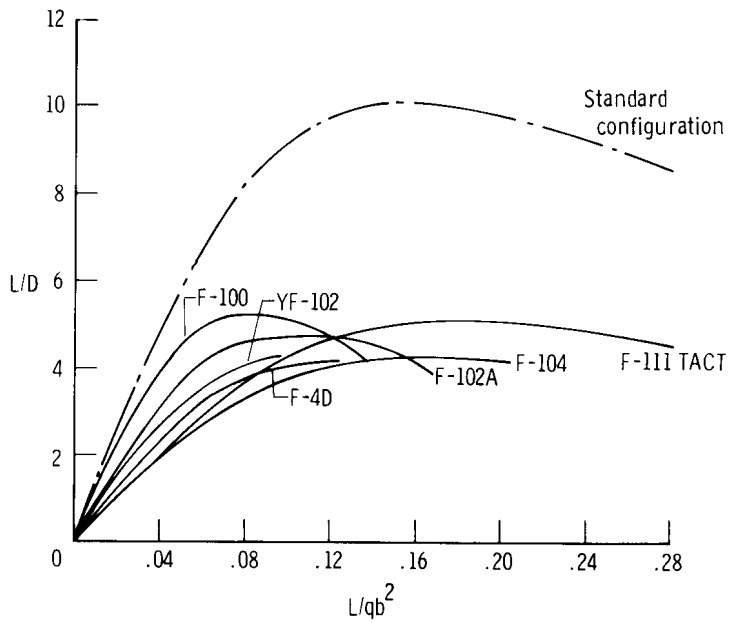
{M = 1.15; h = 10,700 m (35,000 ft); q = 22.10 kN/m² (462 lb/ft²)}

	Configuration						Standard
	F 4D	F 100	YF 102	F-102A	F 104	F 111 TACT	
b, m (ft)	10.20 (33.50)	11.80 (38.58)	11.60 (38.11)	11.60 (38.17)	6.70 (21.94)	10.40 (34.00)	7.47 (24.50)
Λ, deg	-----	-----	-----	-----	-----	58	45
S, m ² (ft ²)	51.7 (557)	35.8 (385)	64.6 (695)	64.6 (695)	18.2 (196)	56.1 (604)	18.6 (200)
S _w , m ² (ft ²)	136.0 (1468)	138.0 (1490)	203.0 (2180)	203.0 (2180)	89.2 (960)	258.0 (2775)	83.6 (900)
S _p , m ² (ft ²)	60.0 (646)	54.8 (590)	77.6 (835)	77.6 (835)	36.4 (392)	105.0 (1135)	29.8 (321)
K	1.14	1.26	1.30	1.30	1.22	1.22	1.40
W _{min} , kN (lb)	70.30 (15,800)	92.50 (20,800)	91.20 (20,500)	91.20 (20,500)	51.15 (11,500)	231.00 (52,000)	-----
W _{max} , kN (lb)	93.4 (21,000)	113.0 (25,400)	121.0 (27,200)	121.0 (27,200)	75.6 (17,000)	356.0 (80,000)	-----
W _{nor} , kN (lb)	77.20 (17,350)	98.75 (22,200)	100.00 (22,500)	100.00 (22,500)	58.30 (13,100)	267.00 (60,000)	44.48 (10,000)
W _{nor} /S, kN/m ² (lb/ft ²)	1.485 (31.0)	3.350 (70.0)	1.555 (32.5)	1.555 (32.5)	3.210 (67.0)	4.790 (100.0)	2.395 (50.0)
qb ² , kN (lb)	2305 (518,300)	3057 (687,400)	2990 (671,000)	2990 (673,000)	989 (222,300)	2375 (533,800)	1240 (279,000)
W _{nor} /qb ²	0.0334	0.0323	0.0340	0.0340	0.0589	0.1124	0.0360
D _o /qb ²	0.01500	0.00803	0.01300	0.01150	0.02040	0.02120	0.00767
S _w /b ²	1.31	1.00	1.50	1.50	2.00	2.40	1.50
T _{max} , kN (lb)	34.15 (7680)	35.35 (7950)	29.35 (6600)	36.50 (8200)	33.35 (7500)	86.70 (19,500)	-----
T _{max} /W _{nor}	0.443	0.358	0.293	0.364	0.573	0.325	-----

(a) C_L versus C_D .(b) L/qb^2 versus D/qb^2 .Figure 13. Comparison of drag polars for century-series fighter aircraft. $M = 1.15$.



(a) L/D versus C_L .



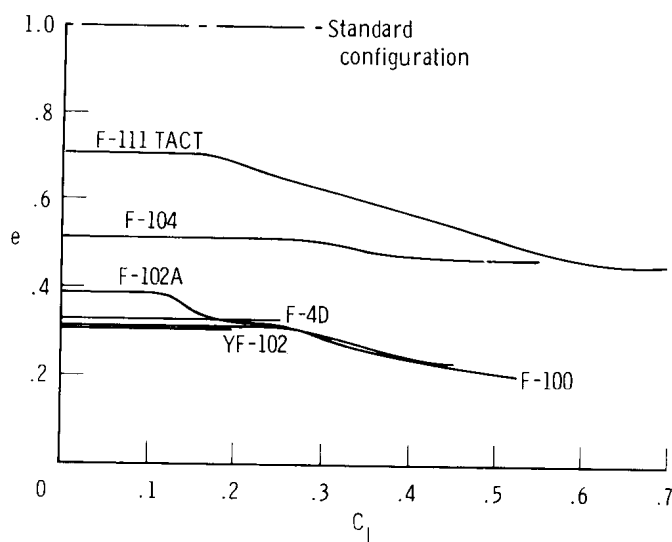
(b) L/D versus L/qb^2 .

Figure 14. Comparison of aerodynamic efficiencies of century-series fighter aircraft. $M = 1.15$.

shows a higher level of efficiency than the YF-102 airplane. Because of the diversity of configurations and reference areas in this series, it is evident that span-squared scaling is required to determine the correct ranking of the aircraft in terms of aerodynamic efficiency.

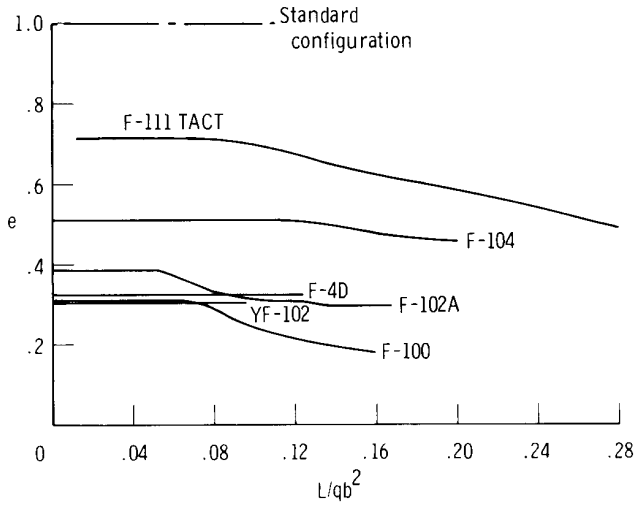
Figure 15 shows that the order of the efficiency factors for the various aircraft is not significantly altered by the conversion from one system to the other. The F-111 TACT airplane with 58° of wing sweep and supercritical airfoil sections shows considerably higher efficiency than the earlier fighter aircraft. Equation (7a) was used to estimate efficiency, assuming $f(m) = 1/\pi$.

In figure 16, the comparative maneuverability of the fighter aircraft is shown to be similar in both systems, except that the F-100 airplane shifts to the highest level in the span-squared notation. This change is attributed to the low span loading of the F-100 airplane (table 2). The F-111 TACT airplane has the highest loading and is therefore the least maneuverable. Thrust limits are noted for the various aircraft in figure 16(b). The YF-102 and F-4D aircraft have insufficient thrust for level flight at a Mach number of 1.15 and an



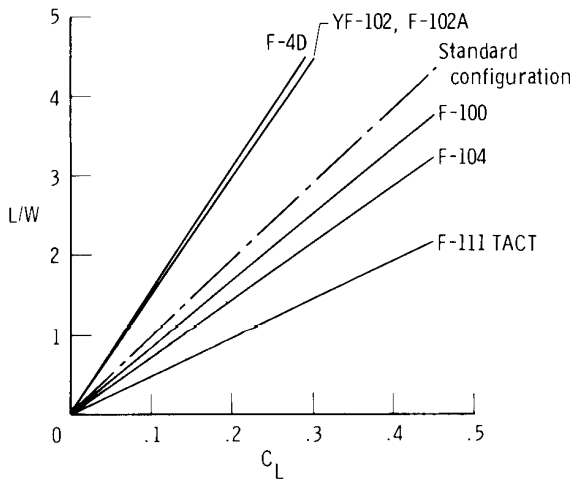
(a) e versus C_L .

Figure 15. Comparison of efficiencies of century-series fighter aircraft. $M = 1.15$.

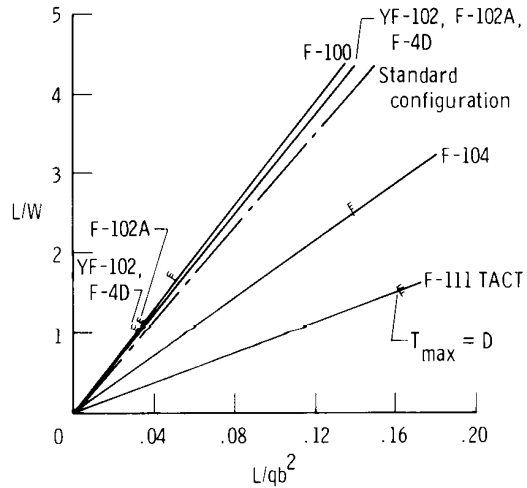


(b) e versus L/qb^2 .

Figure 15. Concluded.



(a) L/W versus C_L .



(b) L/W versus L/qb^2 .

Figure 16. Maneuverability comparison of century-series fighter aircraft. $M = 1.15$; $h = 10,700$ meters (35,000 ft); normal weights (table 2).

altitude of 10,700 meters (35,000 ft). Due to its low thrust limit, the operational maneuverability of the F-100 airplane is about the same as that of the F-111 TACT airplane and much lower than that of the F-104 airplane.

The overall performance characteristics of the fighter aircraft are shown in figure 17. Because of their low thrust levels, the delta-wing aircraft cannot fly at the assumed conditions and the remaining aircraft cannot utilize their full potential. The F-111 TACT airplane has the best overall performance at load factors less than 2.0, whereas the F-100 airplane is best at higher load factors.

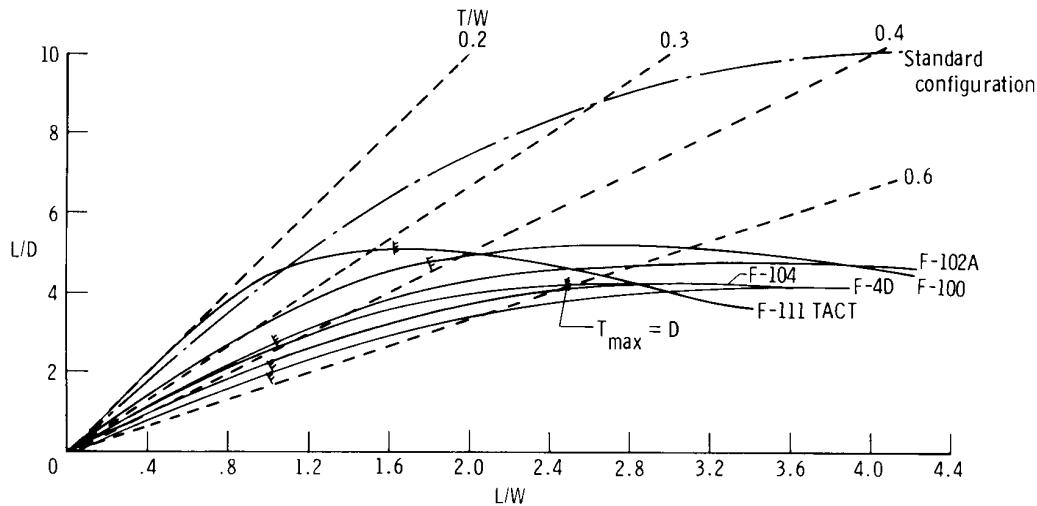
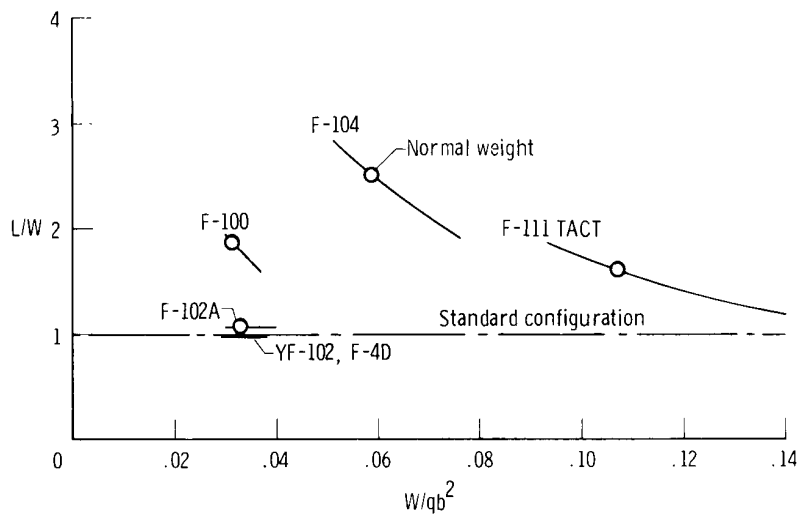


Figure 17. Performance comparison of century-series fighter aircraft. $M = 1.15$; $h = 10,700$ meters (35,000 ft); normal weights (table 2); $D > T_{max}$ for YF-102 and F-4D aircraft.

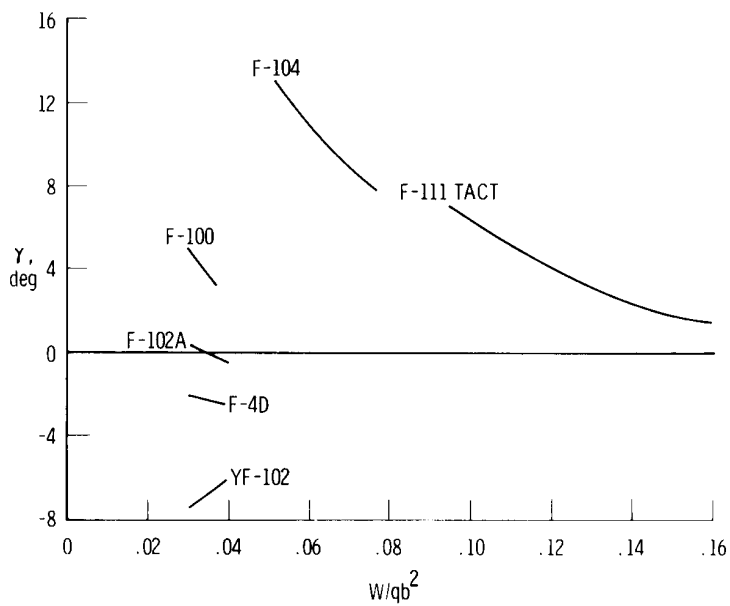
The effect of span loading on maneuverability is shown in figure 18(a). The penalty due to high loading is clearly evident for the F-111 TACT airplane. Similar effects of loading on climb capability are shown in figure 18(b).

F-111A and F-111 TACT Configurations

A comparison of the F-111A and F-111 TACT aircraft is of interest because of the recent introduction of supercritical wings for performance improvements at transonic speeds. The TACT configuration is the same as the basic aircraft except that the outer movable wing panels have been replaced with a new set containing supercritical airfoil sections which provide a larger wing area and smaller span at any given angle of sweep. Sketches of the two aircraft are given in figure 19, and table 3 outlines the principal performance data for wing sweep angles of 26° and 58° for both configurations. These aircraft are compared for a Mach number of 0.90 and an altitude of 3050 meters (10,000 ft). All data were taken from reference 19.



(a) Load factor.



(b) Climb angle.

Figure 18. Effect of span loading on performance of century-series fighter aircraft. $M = 1.15$; $h = 10,700$ meters (35,000 ft); $T_{max} = D$.

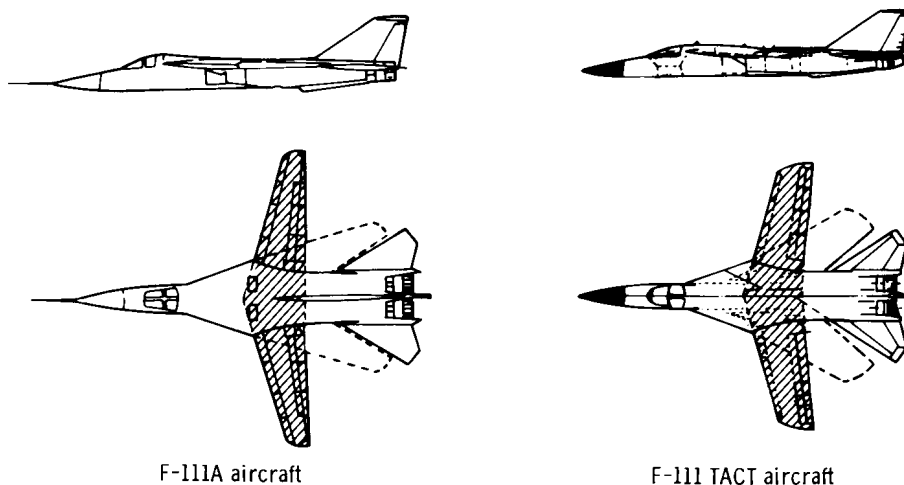


Figure 19. F-111A and F-111 TACT aircraft with reference areas shaded.

TABLE 3.—CHARACTERISTICS OF F-111A AND F-111 TACT AIRCRAFT

[$M = 0.90$; $h = 3048$ m (10,000 ft); $q = 39.5$ kN/m² (825 lb/ft²)]

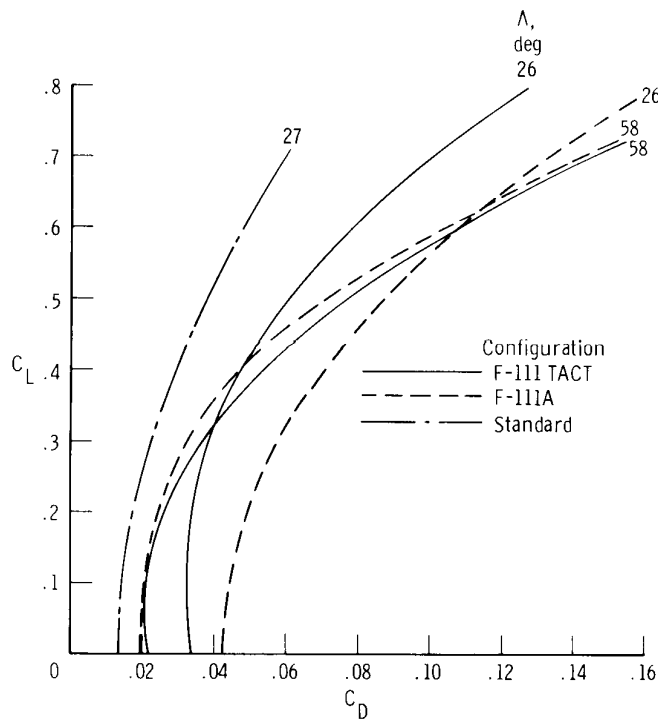
	Configuration				
	F-111A		F-111 TACT	Standard	
	Λ , deg				
	26	58	26	58	27
b , m (ft)	18.6 (61)	11.6 (38)	17.1 (56)	10.4 (34)	12.5 (41)
S_{ref} , m ² (ft ²)	48.8 (525)	48.8 (525)	56.1 (604)	56.1 (604)	46.5 (500)
qb^2 , kN (lb)	13,655 (3,070,000)	5293 (1,190,000)	11,510 (2,587,000)	4242 (953,700)	6147 (1,382,000)
W_{min} , kN (lb)	231 (52,000)	231 (52,000)	231 (52,000)	231 (52,000)	231 (52,000)
W_{max} , kN (lb)	356 (80,000)	356 (80,000)	356 (80,000)	356 (80,000)	356 (80,000)
W_{nor} , kN (lb)	267.0 (60,000)	267.0 (60,000)	267.0 (60,000)	267.0 (60,000)	222.5 (50,000)
W_{nor}/S_{ref} , kN/m ² (lb/ft ²)	5.473 (114.30)	5.473 (114.30)	4.757 (99.35)	4.757 (99.35)	4.788 (100.00)
W_{nor}/qb^2	0.0195	0.0504	0.0232	0.0629	0.0362
D_o/qb^2	0.00592	0.00709	0.00636	0.01126	0.00400
T_{max} , kN (lb)	151 (34,000)	151 (34,000)	151 (34,000)	151 (34,000)	151 (34,000)
T_{max}/W_{nor}	0.567	0.567	0.567	0.567	0.567

It is important to note that rather than treating each angle of sweep as a new configuration, a constant reference area was used for all sweep angles of each version in the original scaling (ref. 19). However, the reference area of the F-111A airplane did not equal that of the F-111 TACT airplane. It is also important to note that rescaling in the span-squared system would require that all the aircraft dimensions be uniformly adjusted to correspond with the unit span for each angle of sweep rather than holding constant the dimensions of all the components except the wing.

The standard configuration chosen for this case was the same as that used for the research aircraft, except that the size, weight, and wing loading were increased to be more nearly comparable to those of the F-111 configurations (table 3). The wing skew angle was kept at 27° , and the method in reference 14 was used for estimating the basic aerodynamic characteristics.

The conventional reference area scaling data shown in figure 20(a) suggest that the performance of the TACT configuration is superior to that of the basic aircraft at low sweep angles and about equal at high sweep angles. In addition, the low sweep angles appear to be more efficient than the high sweep angles in terms of drag due to lift for both configurations. This interpretation would be correct if the F-111A airplane with a fixed angle of sweep (26°) were to serve as the baseline configuration, and if the two configurations had the same reference area. To meet the latter condition, the TACT aircraft data in figure 20(a) were rescaled to the F-111A reference area. The resulting data are shown in figure 20(b). The general arrangement of the polars is not appreciably changed, indicating that the error in conclusions based on figure 20(a) would be small.

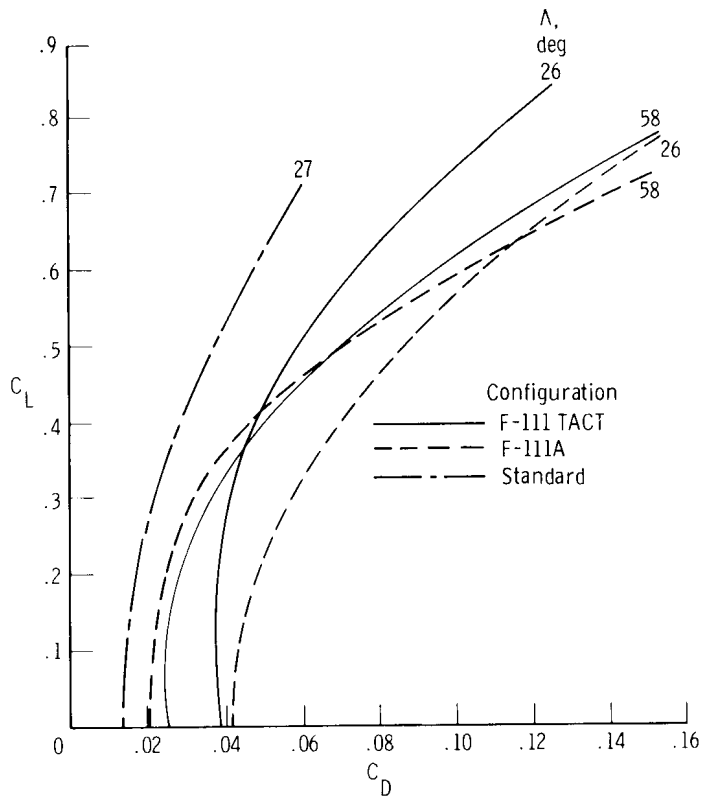
Rescaling the data of figure 20(a) to the span-squared notation changes substantially the order of the various polars, as shown in figure 20(c). For this comparison, the dimensions of all the components of each configuration with various angles of



(a) C_L versus C_D .

Figure 20. Comparison of drag polars for F-111A and F-111 TACT configurations.

$M = 0.90$; $h = 3050$ meters (10,000 ft).



(b) C_L versus C_D . All data scaled to F-111A reference area.

(c) L/qb^2 versus D/qb^2 .

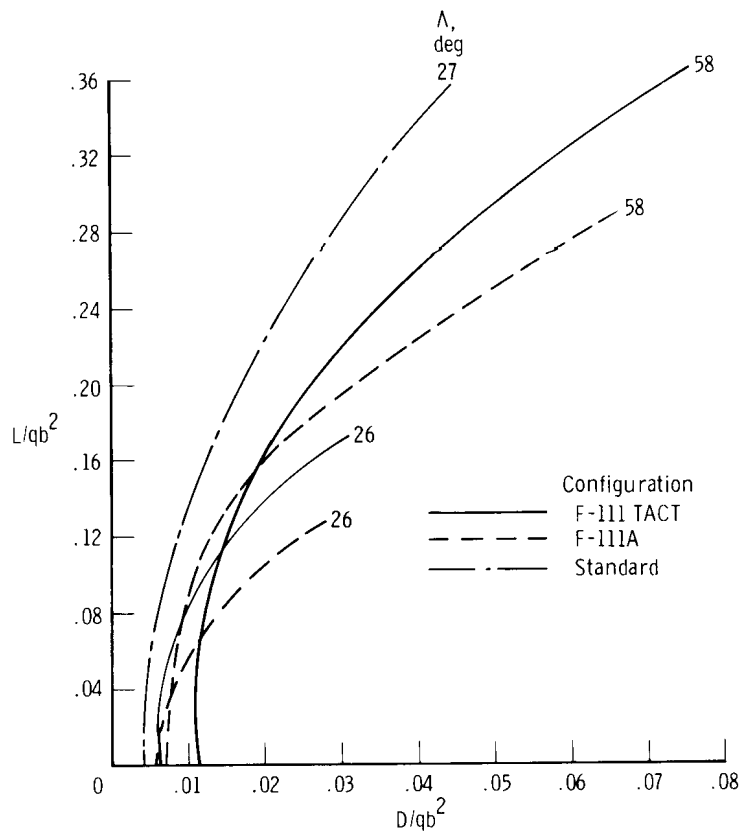
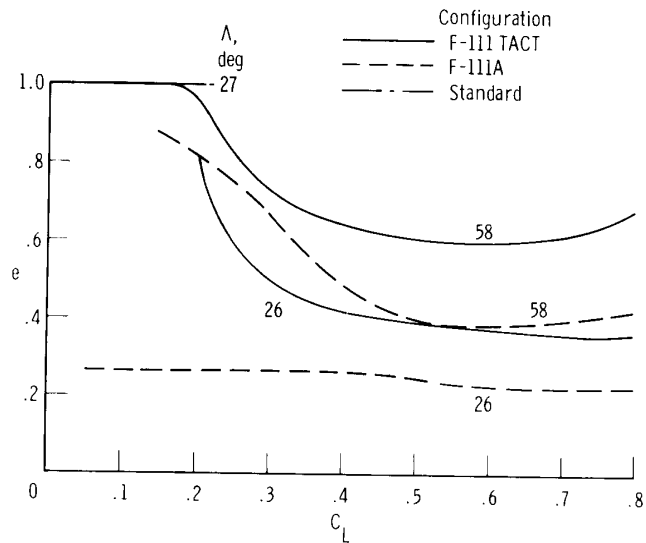
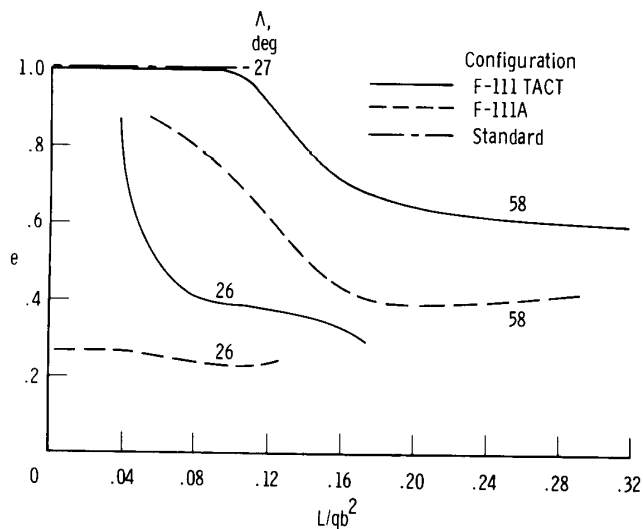


Figure 20. Concluded.

sweep (and therefore various spans) were uniformly transformed to correspond with a common (unit) wingspan. The TACT configuration is now clearly superior not only for low sweep angles, but also for high sweep angles in the upper lift range. In addition, both configurations show improved efficiency with increased sweep angle. Figure 21 shows the corresponding variations of efficiency factor, e , in both notations. The span-squared scaling is presumed to give the correct order of efficiency. Thus, although the fixed reference area method is convenient for



(a) e versus C_L .

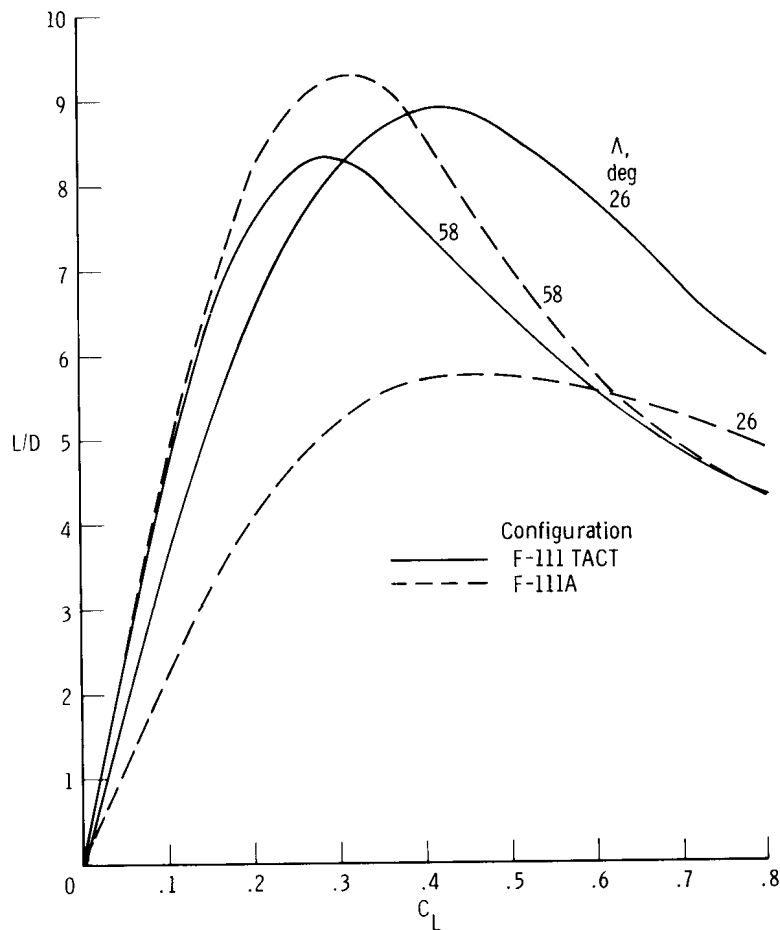


(b) e versus L/qb^2 .

Figure 21. Comparison of efficiency factors for F-111A and F-111 TACT configurations. $M = 0.90$; $h = 3050$ meters (10,000 ft).

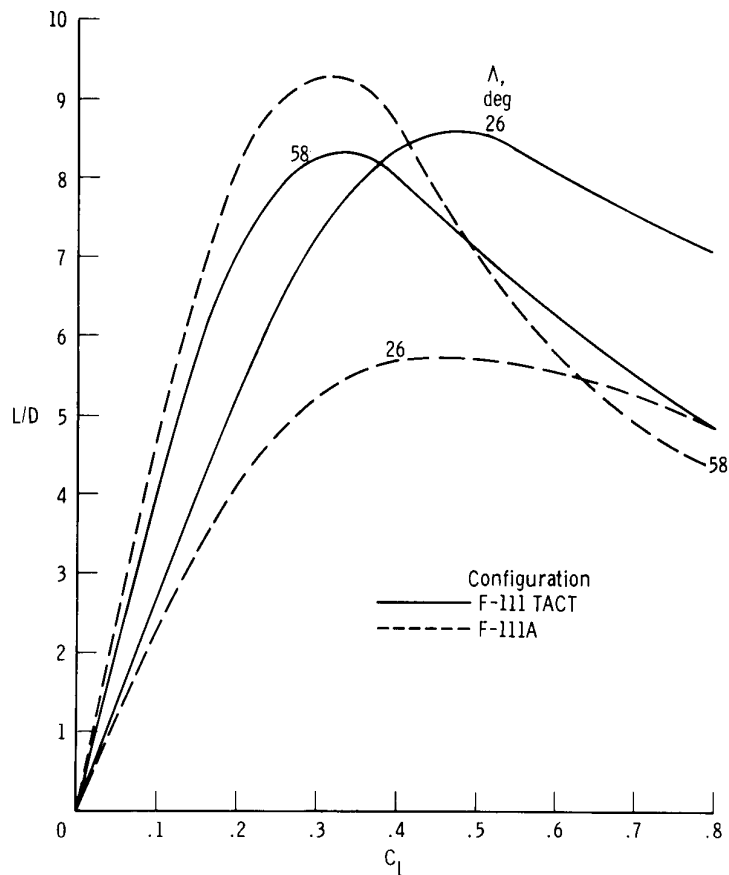
evaluating changes in performance due to alterations of the baseline aircraft, the span-squared approach is more appropriate for determining the basic aerodynamic properties of new configurations.

The lift-to-drag characteristics are shown in figures 22(a) and 22(b), and, like the corresponding drag polars, they are not significantly altered when the data are scaled to the same reference area. At the lower sweep angles, the incremental gain in efficiency due to the supercritical wing panels is substantial. However, the absolute, rather than incremental, measure of efficiency is given by the span-squared representation in figure 22(c). This figure shows the correct order of merit for the various configurations independent of fixed geometric constraints. The configurations with wing sweep angles of 26° now show relatively high lift-to-drag ratios in the low lift range, as would be expected from prior design experience.



(a) L/D versus C_L .

Figure 22. Comparison of aerodynamic efficiencies of F-111A and F-111 TACT configurations. $M = 0.90$; $h = 3050$ meters (10,000 ft).



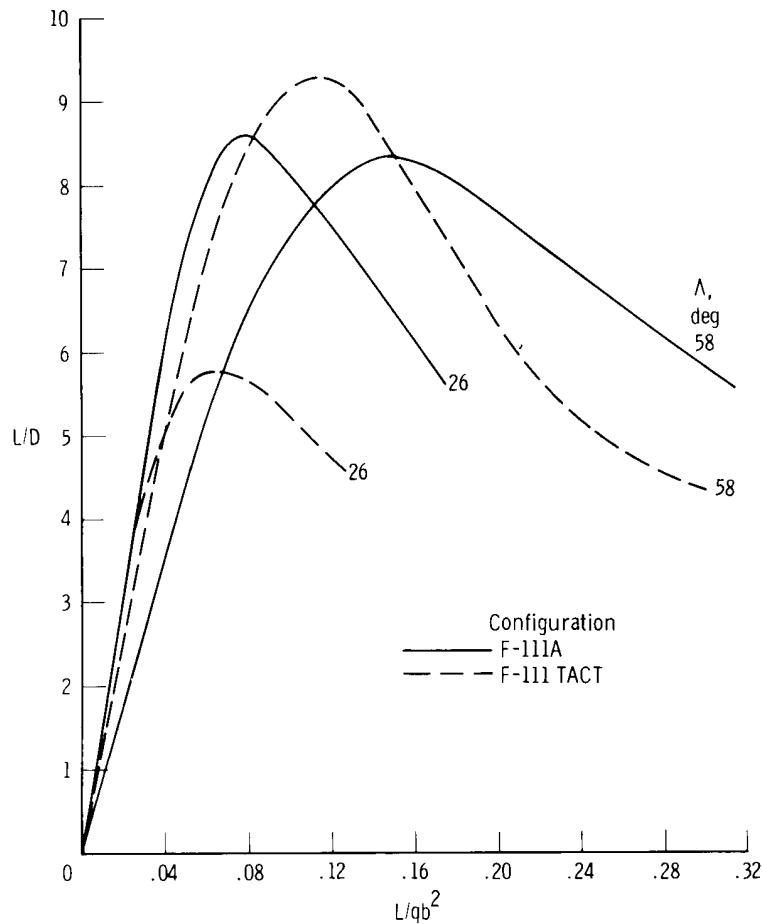
(b) L/D versus C_L . All data scaled to F-111A reference area.

Figure 22. Continued.

Figure 23 shows a performance comparison in terms of load factor. Because the weights of the two aircraft are assumed to be equal, the results in figure 23 are directly proportional to those in figure 22(b) (in other words, $L/W = C_L \div W/qS$).

Therefore, the same deductions would apply. Figure 23, however, also shows thrust-to-weight requirements and performance limitations. The standard configuration, largely due to its comparatively low zero-lift drag, shows much higher performance than the F-111A and F-111 TACT aircraft.

The maximum attainable load factors and climb angles for each configuration are shown in figure 24 for the full range of aircraft weights. A shift of the data for the F-111 TACT aircraft is shown as a correction for the difference in reference areas. For both load factor and climb angle, the shift results in an improved level of performance for the F-111 TACT aircraft. It should be noted that a fixed value of span squared instead of reference area for both aircraft would serve equally well for incremental performance analysis.



(c) L/D versus L/qb^2 .

Figure 22. Concluded.

Lifting Body Series

The lifting body series consists of four experimental, wingless research vehicles (the HL-10, M2-F2, X-24A, and X-24B aircraft), and the F-104 aircraft, which was used for flight training and chase missions. All the research vehicles had more or less triangular-shaped bodies in plan view, were rocket powered, and were used to investigate the subsonic and transonic performance, stability, and control characteristics of this class of aircraft. Sketches of the aircraft in this series are shown in figure 25, and pertinent characteristics are listed in table 4. Data for the series were obtained from references 18 and 20 to 23. Performance comparisons were made at a Mach number of 0.60 and an altitude of 6100 meters (20,000 ft).

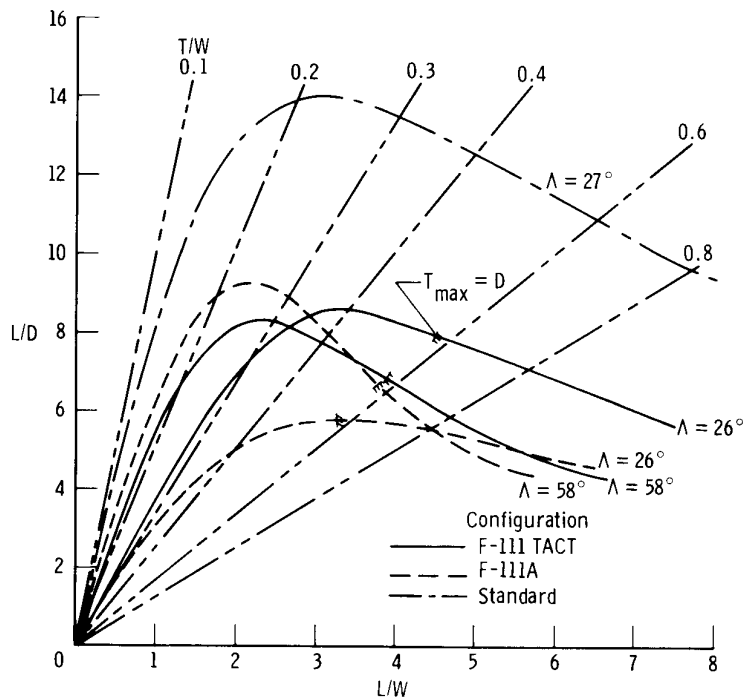


Figure 23. Performance comparison of F-111A and F-111 TACT configurations. $M = 0.90$; $h = 3050$ meters (10,000 ft); normal weights (table 3).

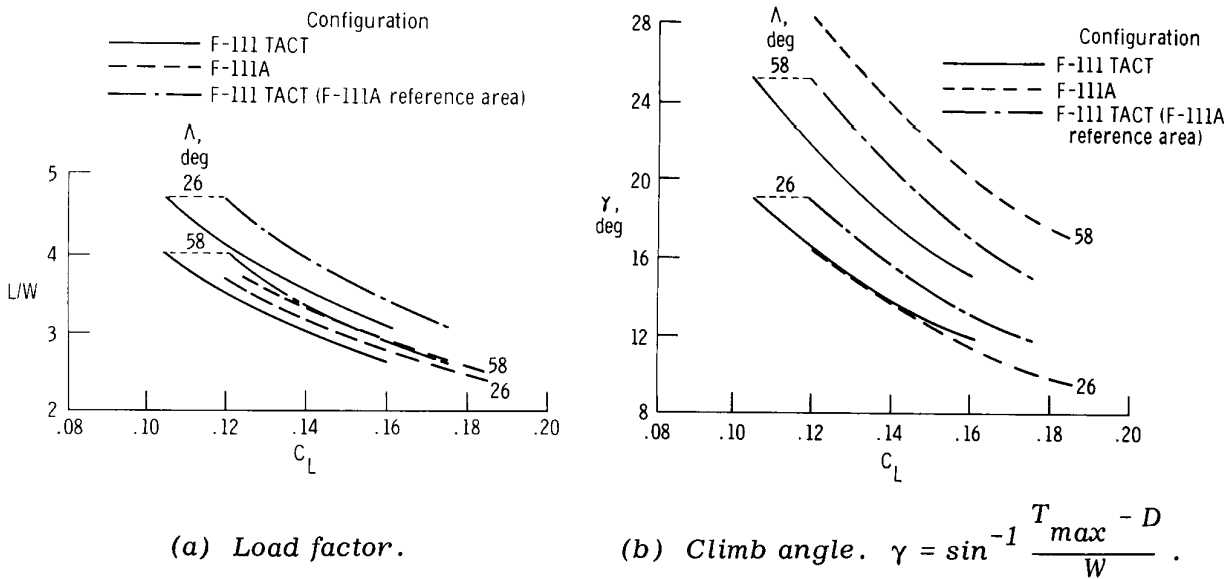


Figure 24. Effect of wing loading on performance of F-111A and F-111 TACT configurations. $M = 0.90$; $h = 3050$ meters (10,000 ft).

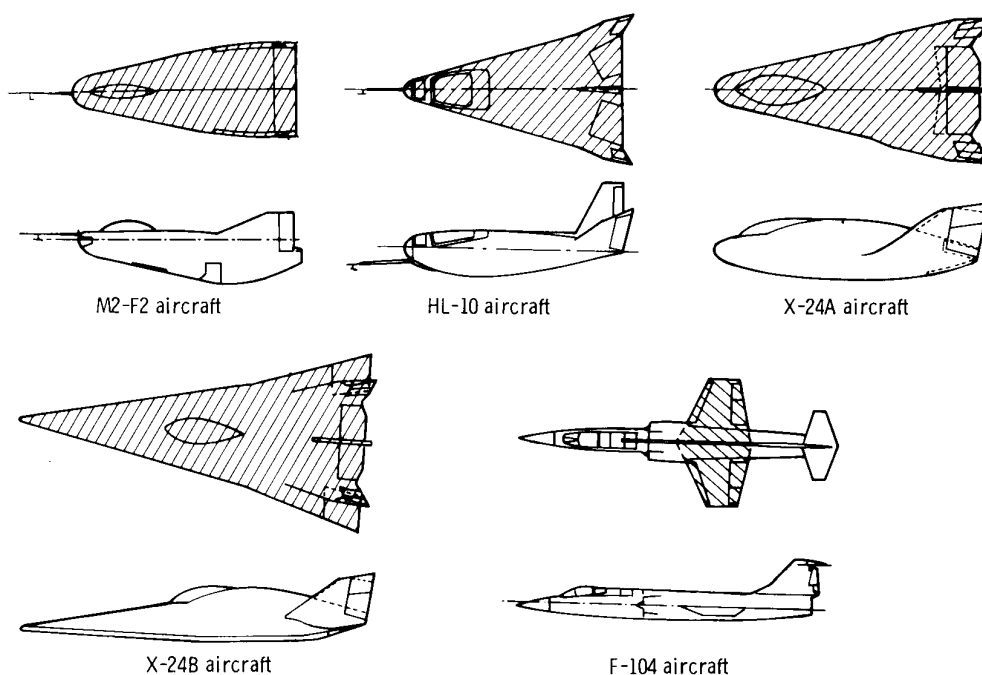


Figure 25. Lifting body series with reference areas shaded.

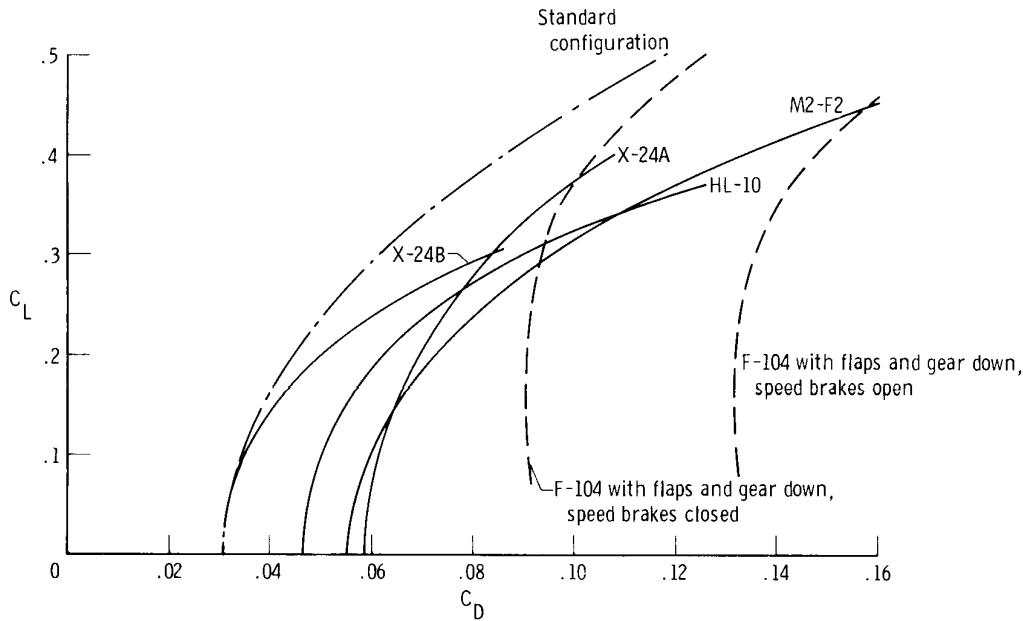
The standard configuration for the lifting body series is assumed to have the same geometry and zero-lift drag, D_o/qb^2 , as the X-24B aircraft. The span loading, however, is assumed to be elliptical ($e = 1$). Pertinent characteristics of this configuration are given in table 4.

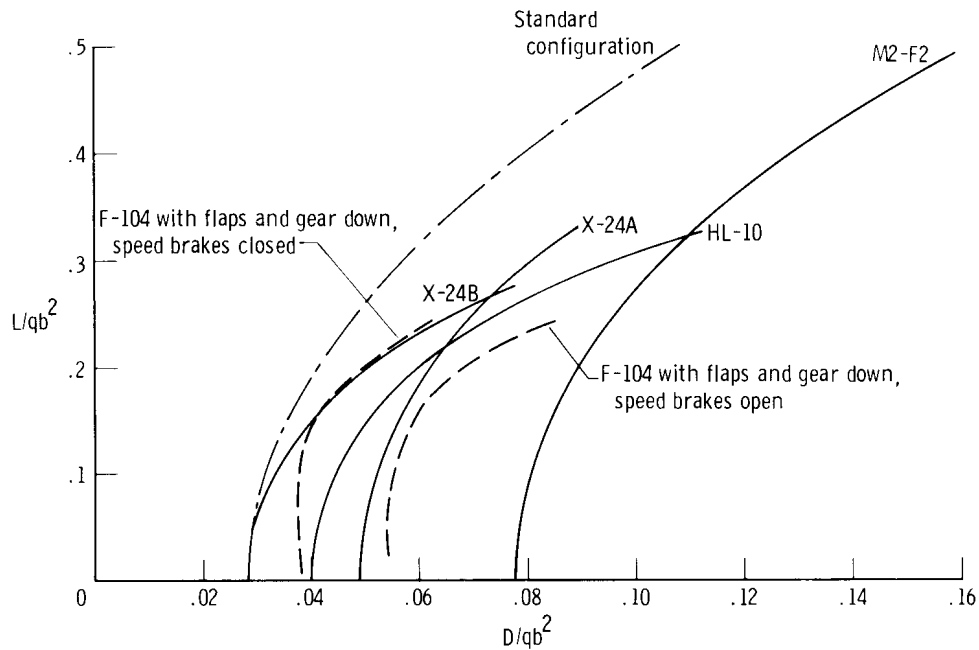
The drag polars for this series in the reference area and span-squared scaling notation are shown in figures 26(a) and 26(b), respectively. These figures show that the relative order of the polars for the HL-10, X-24A, and X-24B aircraft does not change noticeably in the transformation from one system to the other. This result is to be expected since the total planform area is used as the reference area in each case and the planforms are very similar. The exception is the M2-F2 aircraft. Its afterbody tapers inward considerably from a full-length triangular shape, and it exhibits more extensive flow separation than the other aircraft in the series. The data and pilots' comments reported in reference 24 show that, compared with the other lifting bodies, the M2-F2 aircraft exhibits much higher drag and poorer overall flight performance. This trend is not demonstrated by the reference area method (fig. 26(a)), but is quite evident in span-squared notation (fig. 26(b)). It is noteworthy that the two polars for the F-104 airplane (with the flaps and gear down, the speed brakes closed in one case and open in the other) shift to positions that are more representative of the lifting bodies when expressed

TABLE 4. CHARACTERISTICS OF LIFTING BODY SERIES

[$M = 0.60$; $h = 6100$ m (20,000 ft); $q = 11.70$ kN/m² (245 lb/ft²)]

	Configuration						Standard
	HL-10	M2-F2	X-24A	X-24B	F-104 ^a	F-104 ^b	
b , m (ft)	4.15 (13.60)	3.03 (9.95)	4.27 (14.00)	5.79 (19.00)	6.69 (21.94)	6.69 (21.94)	5.79 (19.00)
b^2 , m ² (ft ²)	17.2 (185)	9.2 (99)	18.2 (196)	33.5 (361)	44.7 (481)	44.7 (481)	33.5 (361)
S_{ref} , m ² (ft ²)	14.9 (160.0)	12.9 (139.0)	15.0 (162.0)	30.7 (330.5)	18.2 (196.1)	18.2 (196.1)	30.7 (330.5)
A	1.160	0.712	1.210	1.090	2.450	2.450	1.090
W , kN (lb)	28.50 (6400)	27.35 (6150)	26.70 (6000)	37.80 (8500)	65.40 (14,700)	65.40 (14,700)	33.35 (7500)
W/S , kN/m ² (lb/ft ²)	1.915 (40.0)	2.115 (44.2)	1.770 (37.0)	1.230 (25.7)	3.590 (75.0)	3.590 (75.0)	1.085 (22.7)
qb^2 , kN (lb)	201.6 (45,325)	107.9 (24,255)	213.6 (48,020)	393.4 (88,450)	524.4 (117,900)	524.4 (117,900)	393.4 (88,450)
W/qb^2	0.1410	0.2540	0.1250	0.0960	0.1250	0.1250	0.0848
Upper flap bias, deg	3.0	11.5	19.0	20.0	-----	0.1250	-----
Aileron bias, deg downward	-----	-----	-----	7	-----	-----	-----
Rudder bias, deg-	-----	-----	-----	-----	-----	-----	-----
Outboard	5.0	5.0	-----	-----	-----	-----	-----
Inboard	4.5	-----	10.0	10.0	-----	-----	-----
D_o/qb^2	0.0398	0.0772	0.0483	0.0284	0.0380	0.0547	0.0284

^aFlaps deflected 45°, gear down, speed brakes closed.^bFlaps deflected 45°, gear down, speed brakes open.(a) C_L versus C_D .Figure 26. Comparison of drag polars for lifting body series.
 $M = 0.60$.



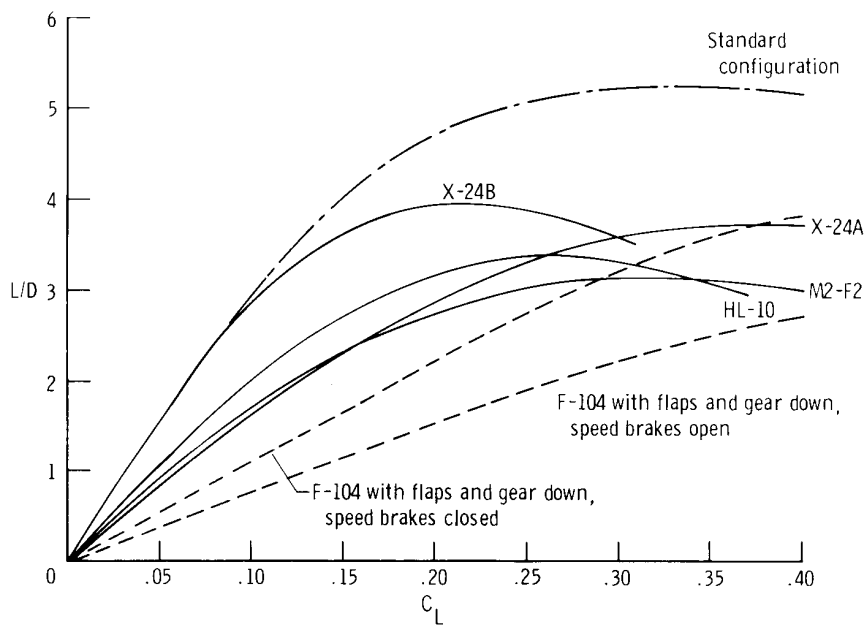
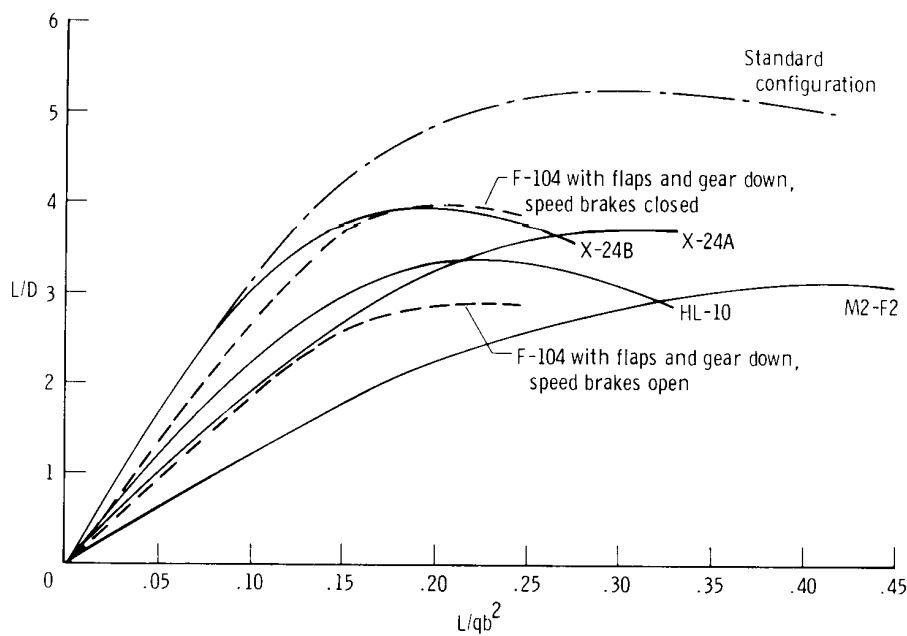
(b) L/qb^2 versus D/qb^2 .

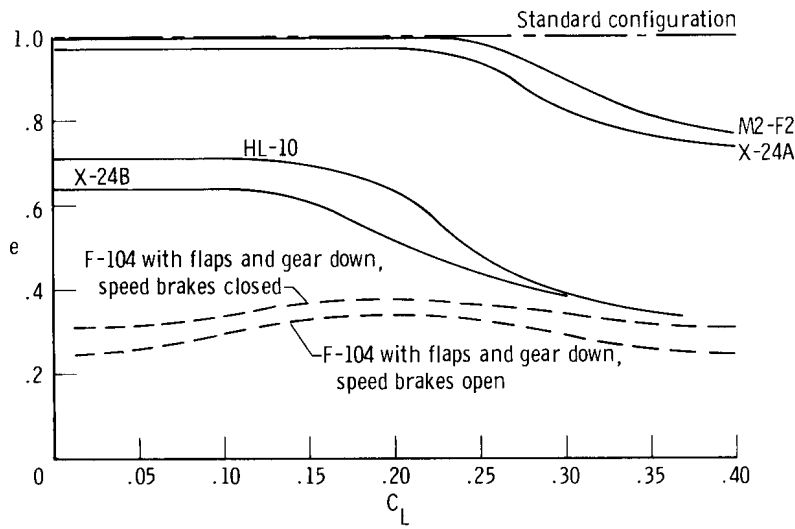
Figure 26. Concluded.

in the span-squared notation. This general agreement has been confirmed by similarities in speed, glide slope, and maneuver characteristics in numerous flights of these aircraft, and by comments from the pilots. The shift of the F-104 polars results from the fact that the aspect ratio (based on the conventional reference area) of the F-104 airplane is much larger than the aspect ratios of the lifting bodies (table 4). Figure 26 also shows that the increments of drag due to lift for the M2-F2 and X-24A aircraft follow more closely the elliptical trend of the standard configuration than do those for the other aircraft.

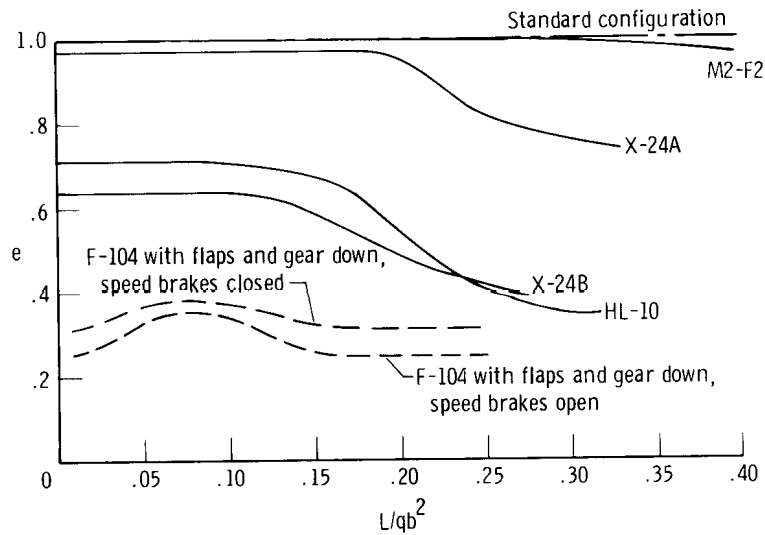
In general, the lift-to-drag characteristics shown in figure 27 exhibit trends similar to those noted earlier for the drag polars. As before, the correct aerodynamic relationship of the various vehicle characteristics is provided by the span-squared scaling rather than the reference area scaling.

The trends of the efficiency factor, e , are presented in figure 28 for the two scaling systems. Relatively little change is observed in the transformation from one system to the other. In figure 28(b), the two configurations that have well rounded bottom contours (the M2-F2 and X-24A aircraft) are nearly 100 percent efficient, whereas the efficiency factors for the HL-10 and X-24B aircraft, which have flatter contours, are noticeably lower than the limit for the standard configuration. The efficiency factor of the F-104 airplane with deflected flaps also departs considerably from the standard.

(a) L/D versus C_L .(b) L/D versus L/qb^2 .Figure 27. Comparison of aerodynamic efficiencies for lifting body series. $M = 0.60$.



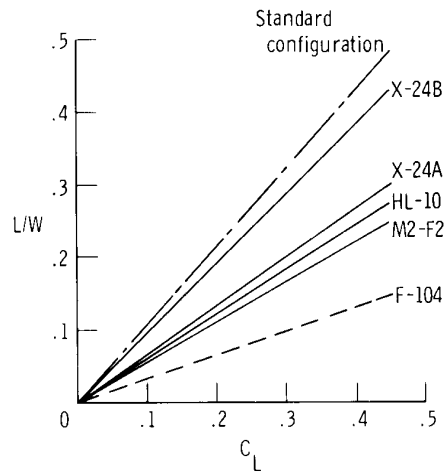
(a) e versus C_L .



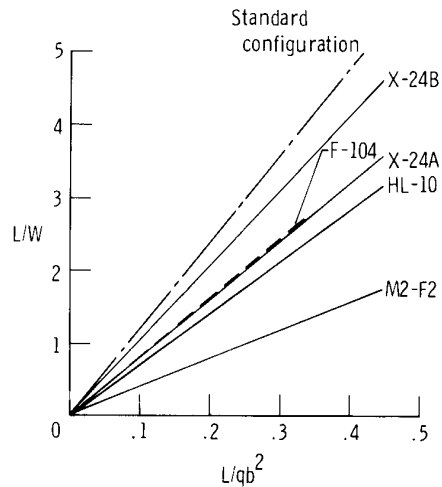
(b) e versus L/qb^2 .

Figure 28. Comparison of efficiency factors for lifting body series. $M = 0.60$.

The HL-10, X-24A, and X-24B aircraft again exhibit the same relative order in both scaling systems in the maneuverability comparison shown in figure 29. However, the M2-F2 aircraft has shifted to the lowest level and the F-104 aircraft to a higher level in the transformation from the conventional to the span-squared method.



(a) L/W versus C_L .



(b) L/W versus L/qb^2 .

Figure 29. Maneuverability comparison for lifting body series. $M = 0.60$.

The overall maneuverability of the series is summarized in figure 30. The X-24A and X-24B aircraft are shown to be superior to the HL-10 and M2-F2 aircraft, and the two configurations of the F-104 airplane encompass quite well the full range of characteristics of the series. The thrust-to-weight ratios for all the configurations (table 4) are sufficiently high to permit operation in the full range of load factors shown in figure 30.

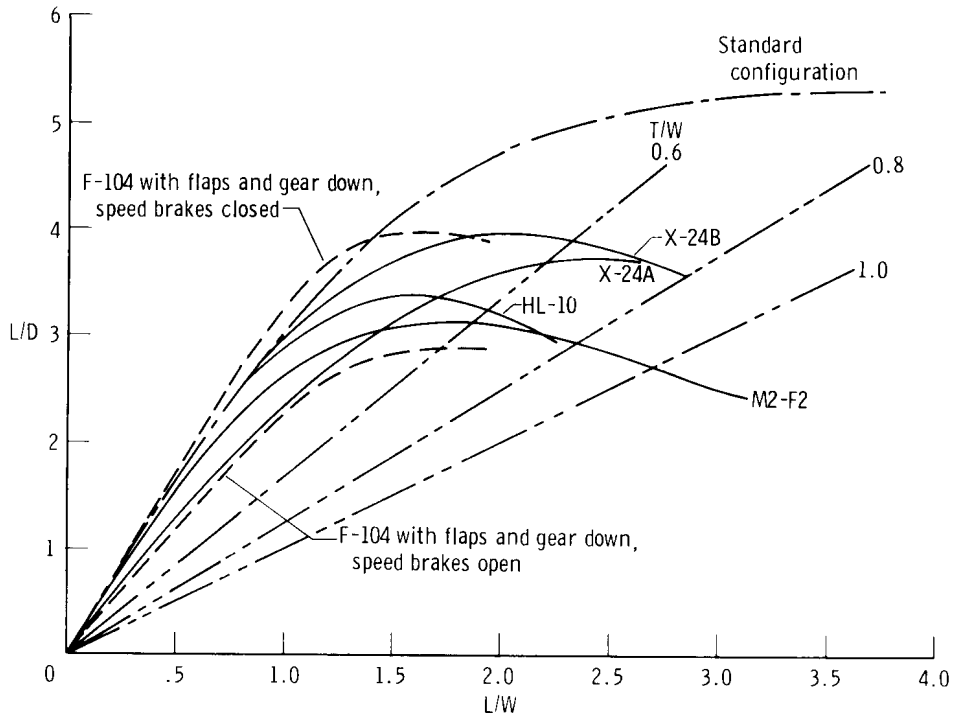


Figure 30. Performance comparison for lifting body series.
 $M = 0.60$.

The maximum lift-to-drag ratios of the series for the flap and control configurations in table 4 range from 3.10 for the M2-F2 aircraft to 3.95 for the X-24B aircraft. The corresponding range of minimum glide slopes extends from about -18° for the M2-F2 aircraft to -14° for the X-24B aircraft.

Supersonic Aircraft

The supersonic group consists of the XB-70, F-111 TACT, F-104, F-106, and B-58 aircraft. These aircraft illustrate the application of span-squared scaling at supersonic Mach numbers for aircraft having widely varying planforms and sizes. Sketches of these aircraft are shown in figure 31, and pertinent characteristics are listed in table 5. All the XB-70 data were obtained with the wingtips deflected downward 65° (not shown in fig. 31). The thickness-to-chord ratios for the group are generally 4° or less, with the exception of the

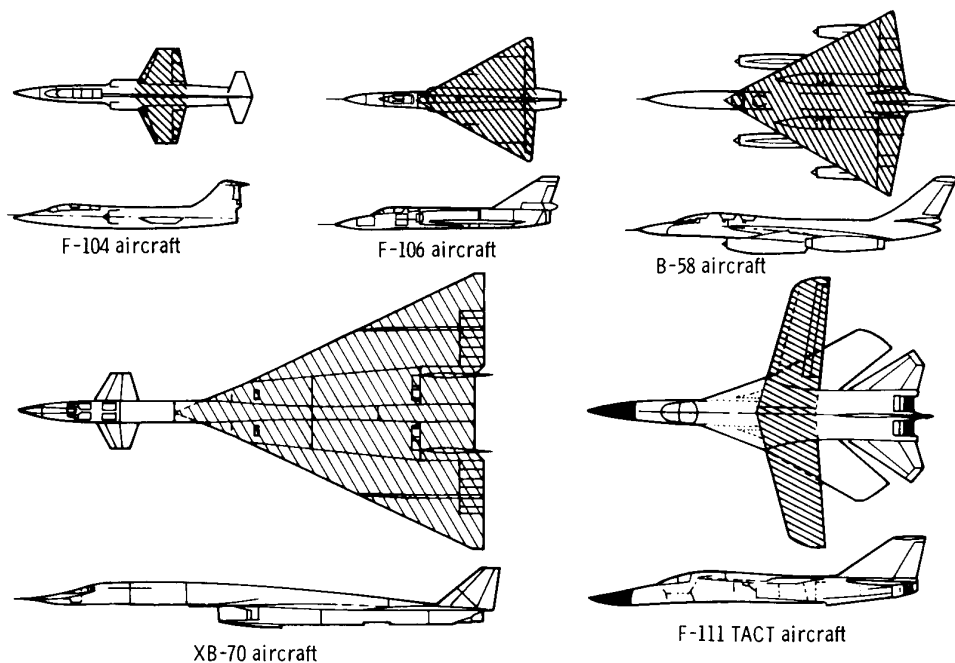


Figure 31. Supersonic aircraft with reference areas shaded.

TABLE 5. - CHARACTERISTICS OF SUPERSONIC AIRCRAFT

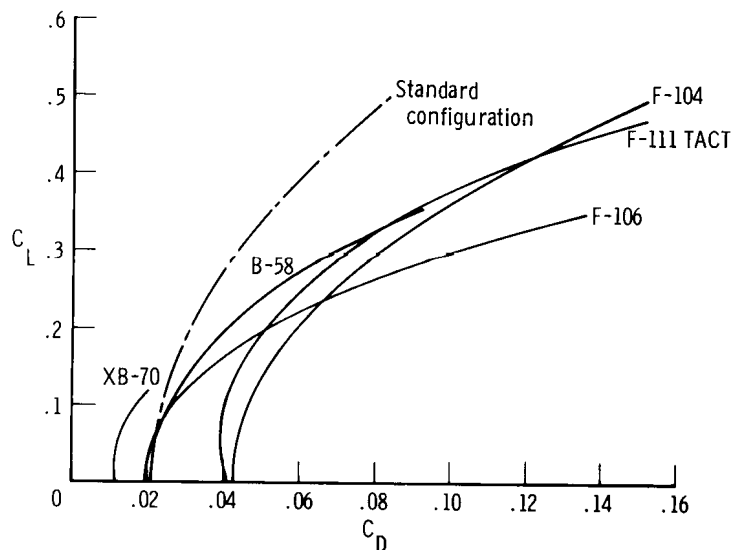
[$M = 2.00$; $h = 13,700$ m (45,000 ft); $q = 41.45$ kN/m² (866 lb/ft²)]

	Configuration					
	F-104	F-106	F-111 TACT	XB-70	B-58	Standard
b , m (ft)	6.69 (21.94)	11.60 (38.13)	10.35 (34.00)	24.70 (81.00)	17.30 (56.83)	16.70 (54.80)
S , m ² (ft ²)	18.2 (196)	64.8 (698)	56.1 (604)	585.0 (6298)	143.0 (1542)	139.0 (1500)
S_w , m ² (ft ²)	89.2 (960)	210.0 (2260)	258.0 (2775)	1580.0 (17,060)	515.0 (5541)	557.0 (6000)
S_p , m ² (ft ²)	36.4 (392)	79.0 (850)	105.0 (1135)	602.0 (6480)	175.0 (1886)	214.0 (2300)
K	1.22	1.33	1.22	1.32	1.47	1.30
W_{min} , kN (lb)	51.15 (11,500)	113.40 (25,500)	231.30 (52,000)	1223.00 (275,000)	249.00 (56,000)	-----
W_{max} , kN (lb)	75.6 (17,000)	157.0 (35,300)	356.0 (80,000)	2445.0 (550,000)	711.7 (160,000)	-----
W_{nor} , kN (lb)	58.5 (13,150)	126.5 (28,440)	269.0 (60,400)	1590.0 (357,500)	388.0 (87,200)	400.0 (90,000)
W_{nor}/S , kN/m ² (lb/ft ²)	3.21 (67.0)	1.85 (38.7)	4.79 (100.0)	2.74 (57.2)	2.79 (58.3)	2.87 (60.0)
qb^2 , kN (lb)	1853 (416,700)	5600 (1,258,000)	4448 (1,000,000)	25,260 (5,679,000)	12,430 (2,796,000)	11,560 (2,600,000)
W_{nor}/qb^2	0.0316	0.0226	0.0604	0.0630	0.0312	0.0347
D_o/qb^2	0.01720	0.00933	0.02150	0.01090	0.01010	0.01050
S_w/b^2	2.00	1.55	2.40	2.23	1.72	2.00
T_{max} , kN (lb)	43.8 (9850)	60.0 (13,500)	133.4 (30,000)	712.0 (160,000)	196.0 (44,000)	-----
T_{max}/W_{nor}	0.749	0.475	0.497	0.448	0.505	-----
A	2.45	2.08	1.91	1.04	2.09	2.00
$f(m)$	1.060	0.900	0.827	0.555	0.905	0.497

inboard sections of the wing for the F-111 TACT aircraft. All performance estimates are based on full afterburner net thrust at a Mach number of 2.00 and an altitude of 13,700 meters (45,000 ft). In this group, only the XB-70 aircraft has a subsonic leading edge at a Mach number of 2.00. Data for the various aircraft were taken from references 18, 19, and 25 to 28.

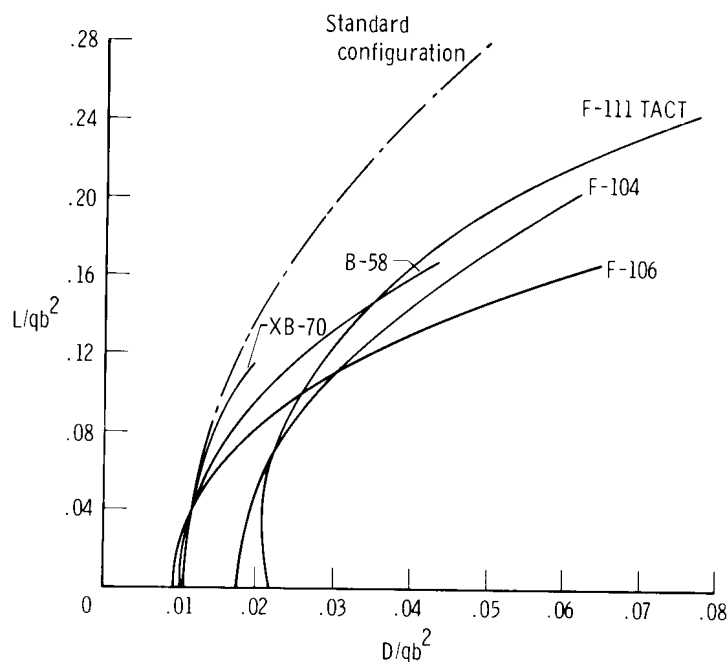
The standard configuration for this group is assumed to have an arrow wing and a blended Sears-Haack fuselage (ref. 1) of the type illustrated in figure 6. A wing aspect ratio of 2.00 was chosen, giving a value of m , or $\beta \cot \Lambda$, of 0.464 (eq. (28)). The induced drag was computed using equations (29a) and (29b), and the zero-lift skin friction and wave drag were determined by the methods of reference 14. A maximum fuselage diameter equal to $b/6$ and a fineness ratio of 8 were selected as being representative of the group. The configuration was sized to be similar to the B-58 airplane. Other pertinent characteristics are given in table 5.

As expected, the polars for the F-106 and B-58 airplanes do not vary significantly between the two scaling systems (fig. 32). Surprisingly, the F-111 TACT airplane also holds a relatively fixed position in relation to the F-106 and B-58 airplanes in the transformation from one system to the other due to the peculiar relationship between the reference area chosen for the configuration with a wing sweep angle of 26° and the reduced span when the sweep angle is increased to 58° . Coincidentally, the reduced aspect ratio for the F-111 TACT airplane (1.91) is nearly equal to the aspect ratios for the F-106 and B-58 airplanes (2.09 for both aircraft). Because its wingtips can be deflected, the XB-70 airplane, like the F-111 TACT airplane, has a varying aspect ratio when a fixed reference area is used. Using the aspect ratio of the XB-70 airplane with its wingtips deflected downward 65° , the XB-70 polar assumes a more appropriate location in the span-squared system. In addition, the XB-70 polar shows the closest agreement with the standard polar.



(a) C_L versus C_D .

Figure 32. Comparison of drag polars for supersonic aircraft. $M = 2.00$.

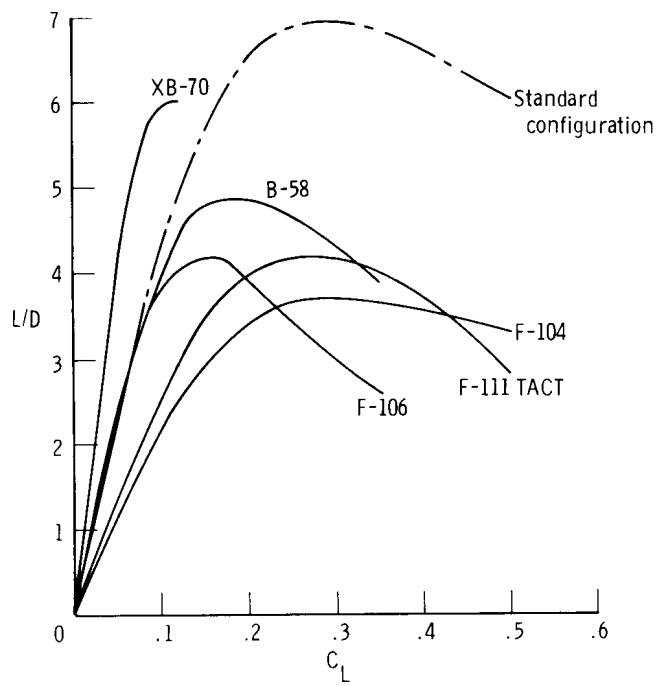


(b) L/qb^2 versus D/qb^2 .

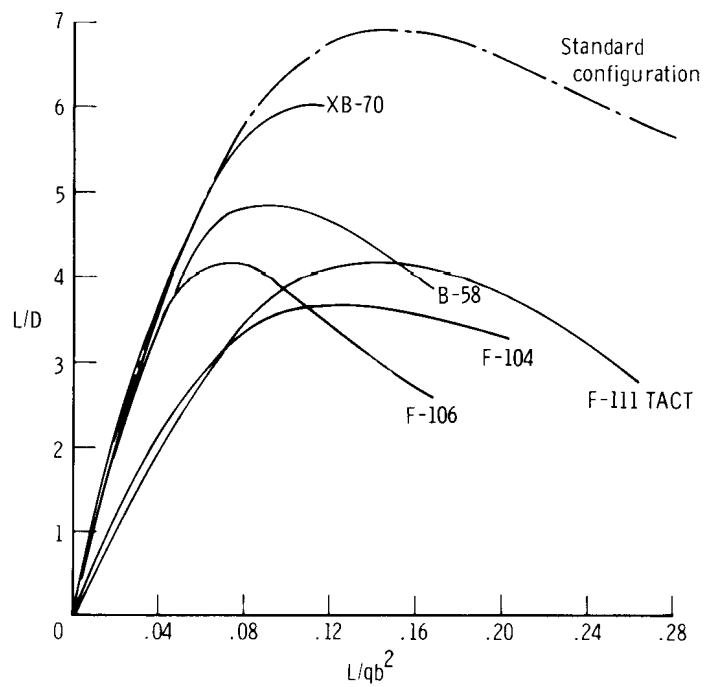
Figure 32. Concluded.

The changes in the trends of the lift-to-drag characteristics between the two methods (figs. 33(a) and 33(b)) are analogous to those of the drag polars in figures 32(a) and 32(b). The two bomber aircraft are shown to be superior to the fighter aircraft. The aerodynamic efficiency of the XB-70 airplane is greater than the efficiencies of the other aircraft and agrees best with the level for the standard configuration.

The efficiency factor for drag due to lift at supersonic speeds is not related simply to $1/\pi$ (eq. (5)) as at subsonic speeds, but has the more complex form $f(m)$ given by equations (7) and (10). The wings of the F-106, B-58, F-104, and F-111 TACT airplanes have supersonic leading edges, and $f(m)$ from equation (10) is equal to $\beta A/4$. The XB-70 wing has subsonic leading edges, and equation (7c) was used to estimate its efficiency factor. The efficiency factors for the supersonic group are shown in figure 34 and are similar in both scaling systems. The F-104 airplane most closely approaches the standard configuration. The efficiency level of the XB-70 airplane with subsonic leading edges is comparable to that of the B-58 airplane but lower than the levels of the F-111 TACT and F-104 airplanes. It is also noteworthy that the efficiency of the F-111 TACT airplane at a Mach number of 2.00 does not differ substantially from its level at a Mach number of 0.90 (fig. 21(b)).

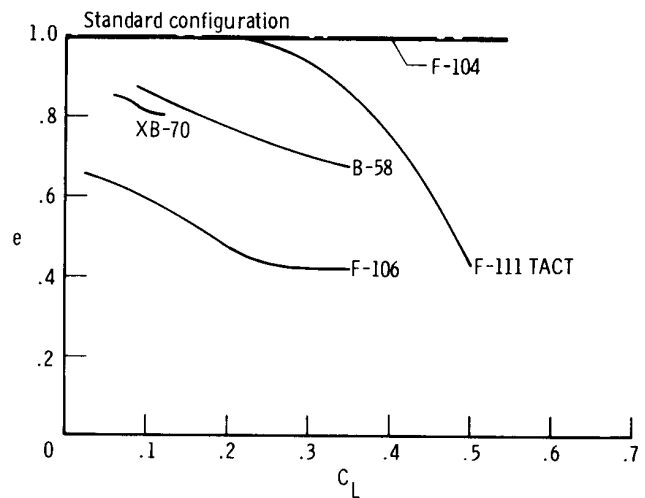


(a) L/D versus C_L .

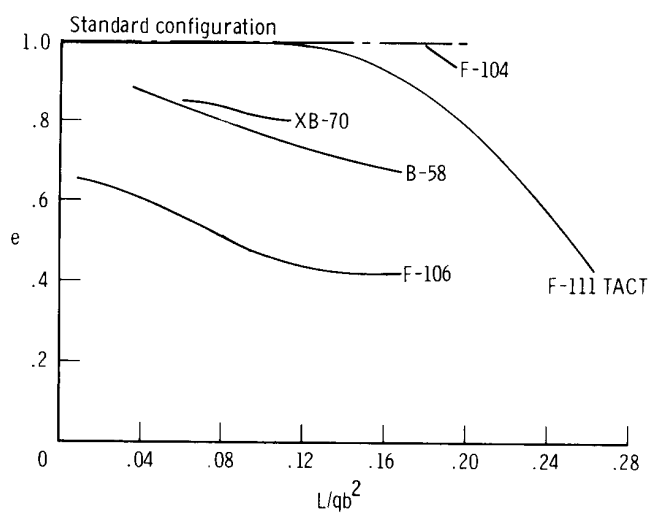


(b) L/D versus L/qb^2 .

Figure 33. Comparison of aerodynamic efficiencies of supersonic aircraft.
 $M = 2.00$.



(a) e versus C_L .



(b) e versus L/qb^2 .

Figure 34. Comparison of efficiency factors for supersonic aircraft. $M = 2.00$.

The effect of vehicle loading on maneuverability is shown in figure 35. The change due to scaling method is significant only in the case of the XB-70 airplane. Both the XB-70 and the F-111 TACT aircraft are comparatively heavy (table 5) and, thus, should be the least maneuverable. This trend is exhibited only in figure 35(b), which represents the span-squared method. Due to its light loading, the B-58 airplane is just as maneuverable as the fighter aircraft. Its attainable load factors, however, do not exceed 2.5 due to limitations in available thrust.

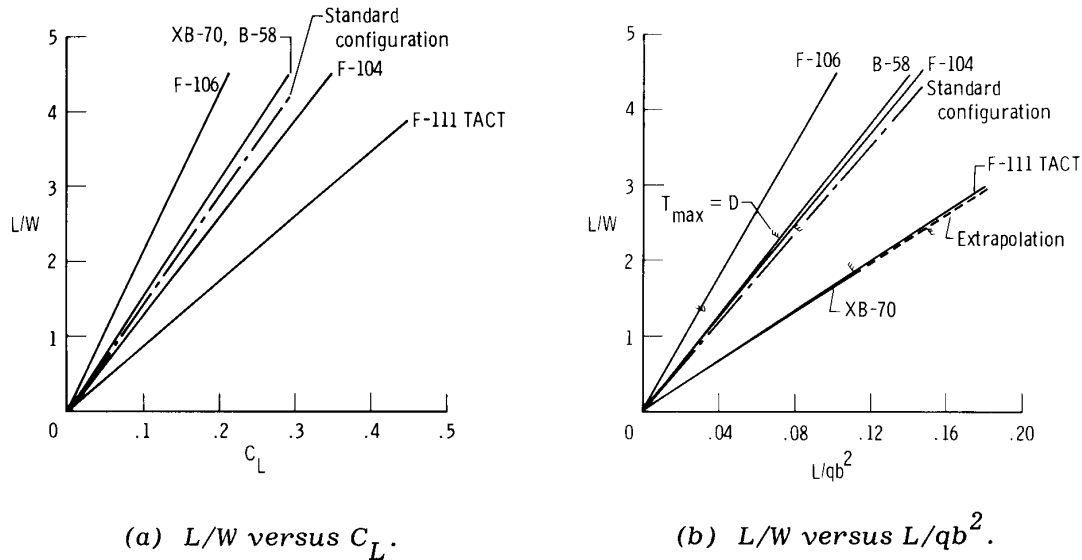


Figure 35. Maneuverability comparison for supersonic aircraft. $M = 2.00$; $h = 13,700$ meters (45,000 ft); normal weights (table 5).

The overall performance of the supersonic aircraft is summarized in figure 36. The heavily loaded F-111 TACT airplane shows a gradual decline in overall performance at the higher (although unattainable) load factors, even though its basic aerodynamic efficiency is moderately high (fig. 34(b)). The flight data for the XB-70 airplane does not extend beyond a load factor of 1.8, but its overall performance is by far superior in the normal range of load factors for transport aircraft. The thrust limit for the XB-70 airplane is beyond the range of the data.

The load factor and climb angle capabilities of the supersonic aircraft for the full range of span loadings are presented in figure 37. The low performance level of the F-106 airplane appears to be due to a combination of low excess thrust and a high level of drag due to lift (fig. 32(b)). The XB-70 airplane shows a relatively high level of performance by virtue of its high excess thrust and subsonic wing leading edges (low drag due to lift). The F-111 TACT airplane also has low drag due to lift but considerably less excess thrust than the XB-70 airplane. The high maneu-

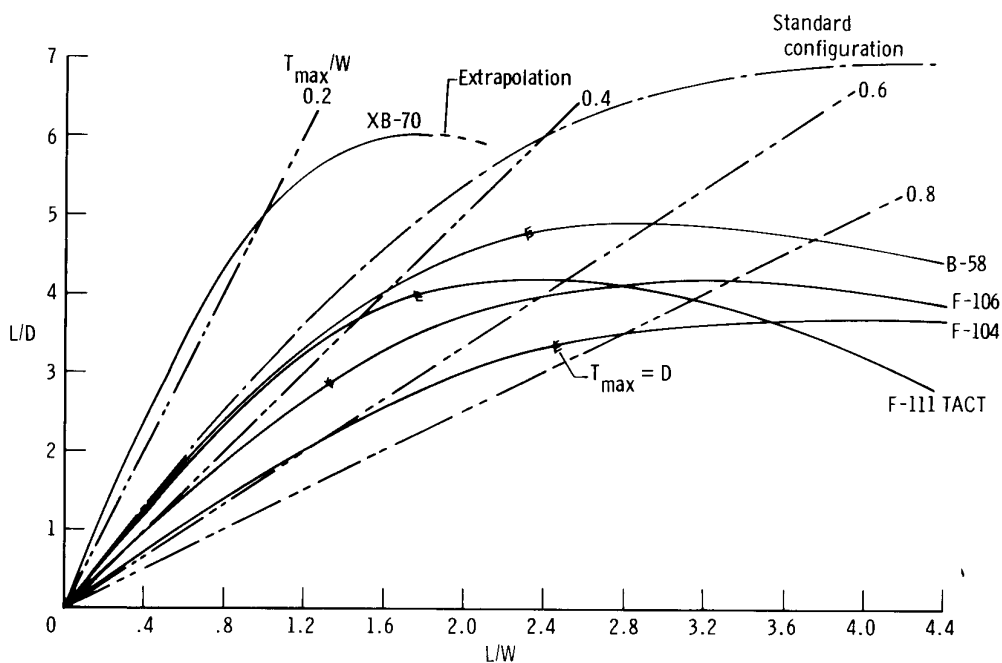
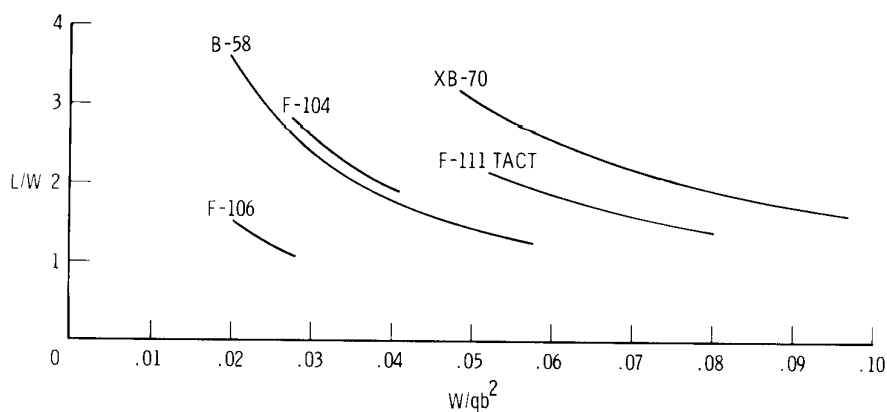
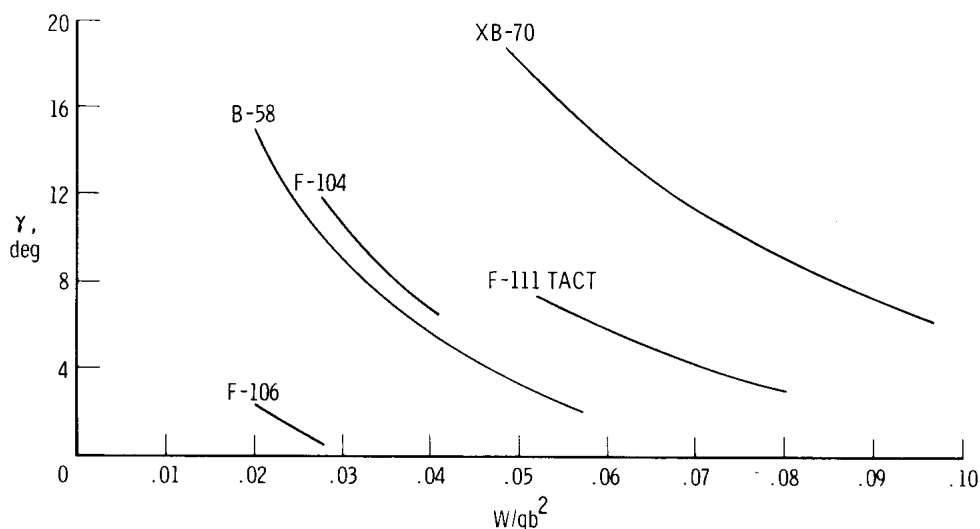


Figure 36. Performance comparison of supersonic aircraft. $M = 2.00$; $h = 13,700$ meters (45,000 ft); normal weights (table 5).



(a) Load factor.

Figure 37. Effect of span loading on performance of supersonic aircraft. $M = 2.00$; $h = 13,700$ meters (45,000 ft); $T_{max} = D$.



(b) Climb angle.

Figure 37. Concluded.

verability of the F-104 and B-58 airplanes is due primarily to their relatively low loading. In general, the two bomber aircraft exhibit better overall performance than the fighter aircraft.

The Mach 2.00 range capability of the group was calculated (eq. (26)) with each aircraft assumed to be fully fueled at its starting point and assumed to have a 5-percent fuel reserve. The principal characteristics for this comparison are listed in table 6. Altitude was adjusted to maintain a constant Mach number of 2.00 with full afterburner thrust (cruise-climb profile). The XB-70 and B-58 ranges

TABLE 6.—CRUISE RANGE CHARACTERISTICS OF SUPERSONIC AIRCRAFT

[M = 2.00]

	Configuration				
	F-104	F-106	F-111 TACT	XB-70	B-58
W_0 , kN (lb)	77.85 (17,500)	178.00 (40,000)	342.50 (77,000)	2558.00 (575,000)	711.70 (160,000)
W_1 , kN (lb)	52.5 (11,800)	116.8 (26,250)	237.3 (53,350)	1290.0 (290,000)	300.0 (67,400)
W_{fuel} , kN (lb)	25.35 (5700)	61.20 (13,750)	105.20 (23,650)	1268.00 (285,000)	411.70 (92,600)
c' , hr ⁻¹	2.22	2.51	2.50	2.45	2.23
L/D	3.200	3.130	3.870	6.015	4.750
$\frac{L/D}{c'}$, hr	1.44	1.25	1.55	2.46	2.13
(L/D) _{max}	3.680	4.170	4.170	6.015	4.840
R, n. mi.	592	543	595	1633	1716
h_0 , m (ft)	17,300 (56,800)	14,000 (46,100)	15,900 (51,800)	14,600 (47,800)	15,400 (50,500)
h_1 , m (ft)	19,800 (65,000)	16,800 (55,100)	18,000 (59,500)	19,000 (62,100)	20,500 (67,500)
W_1/W_0	0.674	0.656	0.693	0.504	0.421

were comparatively high due to their high ratios of L/D to c' and large fuel capacities. Under the assumed conditions, only the XB-70 airplane could be flown near its maximum lift-to-drag ratio. As shown in figure 38, the range capability of the two bomber aircraft was clearly superior to that of the fighter aircraft.

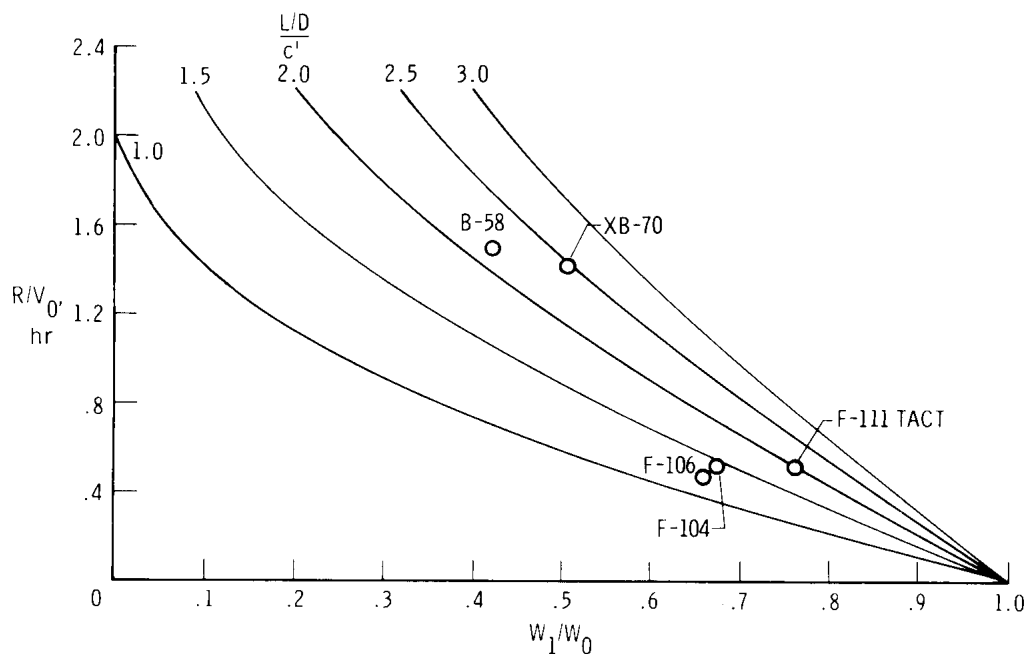


Figure 38. Comparison of range characteristics for supersonic aircraft. $M = 2.00$; 5-percent fuel reserve; $V_0 = 1147$ knots;

$$R/V_0 = 2 \frac{L/D}{c'} \left(1 - \sqrt{\frac{W_1}{W_0}} \right).$$

CONCLUDING REMARKS

The use of the span-squared method for nondimensional aerodynamic scaling in aircraft performance evaluations has been presented as a logical means for avoiding the ambiguities of conventional scaling methods which are based on a somewhat arbitrary wing reference area. A constant wing reference area is shown to be a proper basis for nondimensional comparisons if only the changes in performance due to alterations of a given aircraft are of interest.

By applying span-squared notation, the purely aerodynamic effects on the overall performance of a series of competitive design options can be clearly defined. Aerodynamic, structural, and propulsion efficiencies can then be treated as separate entities in the design and evaluation processes. Thus, deficiencies and areas for

improvement can be defined in more specific terms. Above all, the span-squared approach, as opposed to the reference area method, is more likely to provide a correct assessment of a group of competitive concepts designed to perform a desired mission.

Illustrative applications to several groups of aircraft have revealed interesting trends in the relative performance of past and current designs, and have shown the applicability of the span-squared method. The early research aircraft exhibited similar patterns of aerodynamic efficiency at high subsonic speeds, except for the X-15 aircraft which was designed for a much broader range of research goals. Only the rocket-powered aircraft (the X-1E, D-558-II, and X-15 aircraft), due to their high thrust-to-weight ratios, exhibited high performance capabilities in that early period of high-speed flight research.

The subsequent century-series fighter aircraft displayed a wide range of aerodynamic properties at low supersonic speeds. Lift-to-drag ratio was highest for the F-100 airplane and lowest for the F-104 airplane. At the selected altitude for the performance comparisons, the YF-102 and F-4D aircraft did not perform as well as the other configurations due to inadequate thrust. The F-111 TACT airplane had the best performance at load factors less than 2.0. In addition, the F-111 TACT airplane with its supercritical wing sections was markedly superior to its progenitor, the F-111A airplane, at a Mach number of 0.90 and low angles of wing sweep.

Other than the M2-F2 vehicle, the lifting bodies showed similar trends in aerodynamic efficiency in both scaling systems. Due to its tapered afterbody, the M2-F2 vehicle could be properly assessed only in the span-squared notation. The drag polars of the F-104 airplane were in close agreement with those of the lifting body group when compared on the basis of span squared. This agreement has been confirmed in numerous flight tests where the maneuvering characteristics of the F-104 airplane were shown to be in excellent agreement with those of the lifting bodies.

Finally, the validity of span-squared scaling was illustrated in a performance comparison of several military aircraft of widely varying sizes and configurations at a supersonic Mach number. The two bomber aircraft (the XB-70 and B-58 airplanes) displayed higher lift-to-drag ratios than the three fighter aircraft in the group (the F-104, F-106, and F-111 TACT airplanes). In addition, the overall performance of the two bomber aircraft at an altitude of 13,700 meters (45,000 ft) was comparable to that of the fighter aircraft, and their range capability was far greater than that of the fighter aircraft in a Mach 2 cruise with full afterburner thrust.

Throughout the performance evaluations, a standard configuration was included to give a relative measure of additional gains that might be realized at each flight condition through improved span load distribution and reduced zero-lift drag. The standard configuration in each case was a wing-body combination having elliptic span loading and minimal pressure (wave) drag, but a representative ratio of wetted area (including stabilizing surfaces) to planform area.

Since the mechanism of lift in a fluid medium is basically the same for all lifting elements, it is reasonable to expect that span-squared scaling should apply to all the aerodynamic coefficients (in addition to those for lift and drag) when various aircraft configurations are compared.

*National Aeronautics and Space Administration
Dryden Flight Research Center
Edwards, Calif., December 11, 1978*

APPENDIX

FURTHER SUBSTANTIATION OF SPAN-SQUARED SCALING

The customary relationships for lift and induced drag from various sources are redefined in the span-squared notation in the following sections for subsonic and supersonic flows and for configurations having high slenderness ratios. The examples given are intended to provide further verification of the rationale for using span squared as a basis for performance comparisons of differing aircraft concepts.

Subsonic Flow

It is well known that the induced drag at subsonic speeds is minimal when the spanwise distribution of circulation at large downstream distances (Trefftz plane) is elliptical (refs. 3 and 29). For this case, the downwash velocity, φ , across the span of the vehicle is constant and equal to half the value in the center of the Trefftz plane. In addition, Prandtl (ref. 29) observed that, for a given lift, the required (apparent) mass flow of air with an average downwash velocity, $\bar{\omega}$, is contained in a stream tube having a diameter equal to the span of the aircraft (fig. 39). For this model,

$$L = \bar{\omega}\rho V \frac{\pi b^2}{4} = qb^2 \frac{\pi \bar{\omega}}{2V} \quad (31a)$$

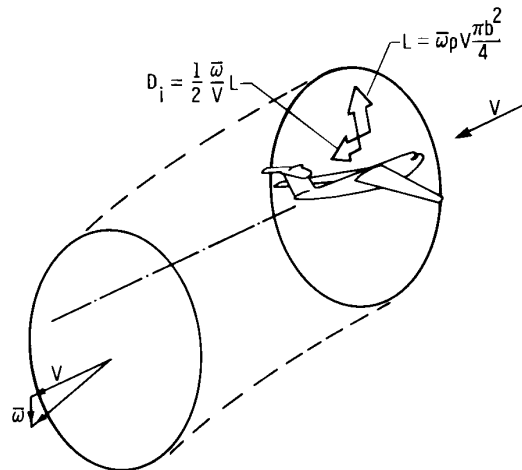


Figure 39. Prandtl apparent mass approximation of lifting vehicle (ref. 4).

$$D_i = \frac{1}{2} \bar{\omega} L = \frac{L^2}{\pi q b^2} \quad (31b)$$

The induced drag is minimal and becomes

$$\frac{D_i}{q b^2} = \frac{1}{\pi} \left(\frac{L}{q b^2} \right)^2 \quad (32)$$

More rigorous methods for calculating lift and induced drag, such as the lifting line approximation (ref. 30), are of the form

$$C_L = A \int_{-1}^1 \left(\frac{\Gamma}{bV} \right)_\eta d\eta \quad (33a)$$

$$C_{D_i} = A \int_{-1}^1 \left(\frac{\Gamma}{bV} \right)_\eta \alpha_\eta d\eta \quad (33b)$$

where η is $2y/b$. Dividing by aspect ratio leads to

$$\frac{L}{q b^2} = \frac{C_L}{A} = \int_{-1}^1 \left(\frac{\Gamma}{bV} \right)_\eta d\eta \quad (34a)$$

$$\frac{D_i}{q b^2} = \frac{C_{D_i}}{A} = \int_{-1}^1 \left(\frac{\Gamma}{bV} \right)_\eta \alpha_\eta d\eta \quad (34b)$$

It is evident that aspect ratio is introduced only as a consequence of defining a set of coefficients based on an arbitrary reference area. Lifting surface methods give similar results (ref. 31).

The drag at zero lift, D_o , arises largely from skin friction of wetted surfaces and, thus, has no direct relationship to span squared. (The small amount of form drag associated with the presence of the boundary layer is neglected in the present analysis.) In the $q b^2$ notation, this drag component is given by

$$\frac{D_o}{q b^2} = C_F \frac{S_w}{b^2} \quad (35)$$

where C_F is the average skin friction coefficient of the surface. The ratio of wetted area to span squared is often used as a measure of design efficiency at zero-lift conditions. Thus, elliptic span loading and minimal wetted area (chordwise dimensions) are fundamental design goals. In practice, however, the surface loading must not reach levels that give rise to premature flow separation and reduced maximum lift.

The total nondimensional drag may now be expressed as

$$\frac{D}{qb^2} = \frac{D_o}{qb^2} + \frac{1}{\pi e} \left(\frac{L}{qb^2} \right)^2 = C_F \frac{S_w}{b^2} + \frac{1}{\pi e} \left(\frac{L}{qb^2} \right)^2 \quad (36)$$

where e is the span efficiency factor customarily used to account for departures from elliptic span loading. This factor is usually given in the form

$$e = \frac{1}{\pi d (D/qb^2) / d (L/qb^2)^2} = \frac{1}{\pi A (dC_D/dC_L^2)} \quad (37)$$

and, for elliptic loading, is equal to unity.

Slender Configurations

Aircraft having slender pointed platforms have been shown by R. T. Jones (ref. 1) to exhibit nearly two-dimensional flow patterns in planes perpendicular to the direction of flight rather than in streamline planes perpendicular to the span of the wing, as illustrated in figure 40.

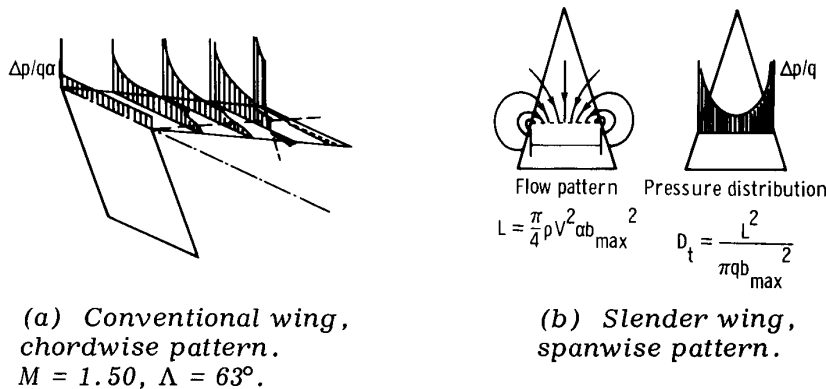


Figure 40. Two-dimensional flow patterns for conventional and slender wing planforms (ref. 1).

The flow is essentially incompressible, and the lift and induced drag are of the form

$$L = \frac{\pi}{4} \rho V^2 \alpha b^2 = \frac{\pi}{2} q \alpha b^2 \quad (38a)$$

$$D_i = \frac{L^2}{\pi q b^2} \quad (38b)$$

The lift and drag occur only as functions of wingspan and are independent of the shape of the wing. The lift distribution is essentially elliptical, and the induced drag is therefore minimal. In nondimensional notation,

$$\frac{L}{q b^2} = \frac{\pi}{2} \alpha \quad (39)$$

The above conditions also apply to nonslender pointed configurations, such as delta- or swept-wing aircraft, operating near the speed of sound subsonically or supersonically. The effect of compressibility (Prandtl-Glauert rule) at this condition is to create a flow pattern similar to that for a long slender wing. Thus, span squared is an appropriate scaling factor for all aircraft operating near the sonic velocity.

In general, slender delta wings with sharp leading edges exhibit a vortex formation that is attributed to flow separation along the leading edges. Reference 32 shows that this separation vortex produces a lift component in addition to the potential lift and appears to have a direct relationship to the leading edge thrust when rotated upward to a position normal to the plane of the wing. The leading edge thrust and, hence, the vortex lift due to its rotation about the leading edge have their roots in the circulation flow system, Γ , about the wing, as discussed in the previous section. Therefore, the vortex lift and its associated lift-induced drag are inherently related to span squared in the same manner as the potential lift (eqs. (34a) and (34b)).

Supersonic Flow

Slender configurations at supersonic speed (that is, configurations with surfaces lying well within the characteristic Mach cones) have properties very similar to those for subsonic speeds, except for the addition of wave drag. A classic example is the oblique elliptic wing concept with leading edges swept well behind the Mach lines (fig. 3). The lift in this case is determined by the subsonic component of flow normal to the wing axis, and the vortex and wave drags are minimized when the wing lift and thickness are distributed elliptically (ref. 1). The total drag is defined as the sum of the friction drag, vortex drag, wave drag due to lift, and wave drag due to volume; that is,

$$D = D_o + \frac{L^2}{\pi q b^2} + \frac{(M^2 - 1)}{2\pi q} \frac{L^2}{\ell^2} + \frac{128q}{\pi} \frac{Q^2}{\ell^4} \quad (40)$$

where b is the span of the oblique wing, and ℓ and Q are the length and volume of the configuration. When $\frac{b}{\cot \Lambda}$ is substituted for ℓ , span squared appears as a basic scaling factor for both the vortex drag and wave drag due to lift. The nondimensional form

$$\frac{D}{qb^2} = C_F \frac{S_w}{b^2} + \frac{1}{\pi} \left(\frac{L}{qb^2} \right)^2 + \frac{m^2}{2\pi} \left(\frac{L}{qb^2} \right)^2 + \frac{128}{\pi} \left(\frac{Q \cot^2 \Lambda}{b^3} \right)^2 \quad (41)$$

where $m = \sqrt{M^2 - 1} (\cot \Lambda)$, is analogous to the subsonic expression except for the addition of wave drag.

In general, the lift and drag due to lift of supersonic configurations with subsonic leading edges are dependent only on the sweep of the leading edge in relation to the Mach lines. A representative case is the triangular wing for which

$$C_L = \frac{\pi A \alpha}{2E'(m)} \quad (42a)$$

$$C_{D_i} = \frac{\pi A \alpha^2}{2E'(m)} \left[1 - \frac{\sqrt{1 - m^2}}{2E'(m)} \right] \quad (42b)$$

where

$$m = \frac{\cot(\text{leading edge sweep angle})}{\cot(\text{sweep angle of Mach lines})} = \beta \cot \Lambda \quad (42c)$$

and $E'(m)$ is the elliptic integral (second kind) of $\sqrt{1 - m^2}$ (ref. 1). Dividing by aspect ratio gives

$$\frac{L}{qb^2} = \frac{\pi \alpha}{2E'(m)} \quad (43a)$$

$$\frac{D_i}{qb^2} = \frac{\pi \alpha^2}{2E'(m)} \left[1 - \frac{\sqrt{1 - m^2}}{2E'(m)} \right] \quad (43b)$$

$$= \frac{1}{\pi} \left[2E'(m) - \sqrt{1 - m^2} \right] \left(\frac{L}{qb^2} \right)^2$$

Both expressions are independent of surface area and are consistent with the slender wing result as m approaches zero.

The lift and drag due to lift of configurations having supersonic leading edges, however, are directly dependent on the affected surface areas (hence, also aspect ratio). The rectangular wing is the simplest example where (ref. 1)

$$C_L = \frac{4\alpha}{\beta} \left(\frac{\beta A - 1/2}{\beta A} \right) \quad (44a)$$

$$\frac{C_{D_i}}{C_L^2} = \frac{\beta^2 A}{4\beta A - 2} \quad (44b)$$

In the qb^2 notation,

$$\frac{L}{qb^2} = \frac{4\alpha}{\beta A} \left(\frac{\beta A - 1/2}{\beta A} \right) \quad (45a)$$

$$\frac{D_i}{qb^2} = \left(\frac{L}{qb^2} \right)^2 \frac{(\beta A)^2}{4\beta A - 2} \quad (45b)$$

The wave drag at zero lift (due to thickness) is also functionally related to surface area. For wings with either subsonic or supersonic leading edges (ref. 14),

$$C_{D_w} S_{ref} \approx \left[\left(\frac{t'}{c} \right)_{eff} \right]^2 S_w \quad (46)$$

and for slender bodies,

$$C_{D_w} S_{ref} \approx f_n^2 S_B \quad (47)$$

where $\left(\frac{t'}{c} \right)_{eff}$ is the effective thickness-to-chord ratio, f_n is the body fineness ratio, S_w is the wing area producing wave drag, and S_B is the maximum body cross-sectional area. In the qb^2 notation, for wings

$$\frac{D_w}{qb^2} \approx \left[\left(\frac{t'}{c} \right)_{eff} \right]^2 \frac{S_w}{b^2} \quad (48a)$$

and for bodies

$$\frac{D_w}{qb^2} \approx f_n^2 \frac{S_B}{b^2} \quad (48b)$$

where $\frac{S_w}{b^2}$ and $\frac{S_B}{b^2}$ are analogous to the wetted area term, $\frac{S_w}{b^2}$, as a measure of aerodynamic efficiency.

In summary, span squared appears in theory to be a consistent and unambiguous scaling factor for correlation of the lift and induced drag of aircraft having all leading edges subsonic. In addition, it provides a useful basis for assessing aerodynamic efficiency at zero lift.

REFERENCES

1. Ames Research Center: Collected Works of Robert T. Jones. NASA TM X-3334, 1976.
2. Mechtly, E. A.: The International System of Units-Physical Constants and Conversion Factors. Second Revision. NASA SP-7012, 1973.
3. Munk, Max M.: The Minimum Induced Drag of Aerofoils. NACA Rept. 121, 1921.
4. Couch, Lana M.; and Brooks, Cuyler W., Jr.: Effect of Blockage Ratio on Drag and Pressure Distributions for Bodies of Revolution at Transonic Speeds. NASA TN D-7331, 1973.
5. Walker, Harold J.; and Wolowicz, Chester H.: Theoretical Stability Derivatives for the X-15 Research Airplane at Supersonic and Hypersonic Speeds Including a Comparison With Wind-Tunnel Results. NACA TM X-287, 1960.
6. Van Dyke, Milton D.: A Study of Hypersonic Small-Disturbance Theory. NACA Rept. 1194, 1954.
7. Bellman, Donald R.: A Summary of Flight-Determined Transonic Lift and Drag Characteristics of Several Research Airplane Configurations. NASA MEMO 3-3-59H, 1959.
8. Bellman, Donald R.; and Sisk, Thomas R.: Preliminary Drag Measurements of the Consolidated Vultee XF-92A Delta-Wing Airplane in Flight Tests to a Mach Number of 1.01. NACA RM L53J23, 1954.
9. Carman, L. Robert; and Carden, John R.: Lift and Drag Coefficients for the Bell X-1 Airplane (8-Percent-Thick Wing) in Power-Off Transonic Flight. NACA RM L51E08, 1951.
10. Bellman, Donald R.; and Murphy, Edward D.: Lift and Drag Characteristics of the Douglas X-3 Research Airplane Obtained During Demonstration Flights to a Mach Number of 1.20. NACA RM H54I17, 1954.
11. Bellman, Donald R.: Lift and Drag Characteristics of the Bell X-5 Research Airplane at 59° Sweepback for Mach Numbers From 0.60 to 1.03. NACA RM L53A09c, 1953.
12. Nugent, Jack: Lift and Drag Characteristics of the Douglas D-558-II Research Airplane Obtained in Exploratory Flights to a Mach Number of 2.0. NACA RM L54E03, 1954.

13. Saltzman, Edwin J.; and Garringer, Darwin J.: Summary of Full-Scale Lift and Drag Characteristics of the X-15 Airplane. NASA TN D-3343, 1966.
14. USAF Stability and Control DATCOM. Air Force Flight Dynamics Lab., Wright-Patterson Air Force Base, Oct. 1960 (rev. Apr. 1978).
15. Saltzman, Edwin J.; and Asher, William P.: Transonic Flight Evaluation of the Effects of Fuselage Extension and Indentation on the Drag of a 60° Delta-Wing Interceptor Airplane. NACA RM H57E29, 1957.
16. Rolls, L. Stewart; and Wingrove, Rodney C.: An Investigation of the Drag Characteristics of a Tailless Delta-Wing Airplane in Flight, Including Comparison With Wind-Tunnel Data. NASA MEMO 10-8-58A, 1958.
17. Nugent, Jack: Lift and Drag of a Swept-Wing Fighter Airplane at Transonic and Supersonic Speeds. NASA MEMO 10-1-58H, 1959.
18. Marshall, Robert T.; and Schweikhard, William G.: Modeling of Airplane Performance From Flight-Test Results and Validation With an F-104G Airplane. NASA TN D-7137, 1973.
19. Cooper, James M., Jr.; Hughes, Donald L.; and Rawlings, Kenneth, III: Transonic Aircraft Technology-Flight-Derived Lift and Drag Characteristics. Volume I of II. AFFTC-TR-77-12, Air Force Flight Test Center, Edwards Air Force Base, July 1977.
20. Pyle, Jon S.; and Swanson, Robert H.: Lift and Drag Characteristics of the M2-F2 Lifting Body During Subsonic Gliding Flight. NASA TM X-1431, 1967.
21. Pyle, Jon S.: Lift and Drag Characteristics of the HL-10 Lifting Body During Subsonic Gliding Flight. NASA TN D-6263, 1971.
22. Ash, Lawrence G.: Flight Test and Wind Tunnel Performance Characteristics of the X-24A Lifting Body. Volume I of II. FTC-TD-71-8, Air Force Flight Test Center, Edwards Air Force Base, June 1972.
23. Richardson, David F.: Comparison of Flight Test and Wind Tunnel Performance Characteristics of the X-24B Research Aircraft. AFFTC-TR-76-10, Air Force Flight Test Center, Edwards Air Force Base, Apr. 1976.
24. Flight Test Results Pertaining to the Space Shuttlecraft. NASA TM X-2101, 1970.
25. Craig, R. E.; Jackson, J. T.; and Oesterle, D. S.: F-106A Aerodynamic and Propulsion Data for USAF Energy-Maneuverability Program. GDC-DCD-68-006, General Dynamics, July 1968.
26. Fox, M. K.; and Wadsworth, E. A.: Correlation of the Supersonic Thrust and Drag of the B-58A Airplane. FZA-4-415, General Dynamics, 20 Dec. 1963.

27. Arnaiz, Henry H.: Flight-Measured Lift and Drag Characteristics of a Large, Flexible, High Supersonic Cruise Airplane. NASA TM X-3532, 1977.
28. Michaels, J. M.; Fisk, W. S.; McManus, H. L.; and Henderson, R. L.: Estimated Performance Graphic Presentation: YJ93-GE-3 Turbojet Engine. R61FPD321, General Electric, Sept. 1961.
29. Tietjens, O. G.: Applied Hydro- and Aeromechanics: Based on Lectures of L. Prandtl, Ph. D. Dover Publications, Inc., New York, 1957.
30. DeYoung, John; and Harper, Charles W.: Theoretical Symmetric Span Loading at Subsonic Speeds for Wings Having Arbitrary Plan Form. NACA Rept. 921, 1948.
31. Margason, Richard J.; and Lamar, John E.: Vortex-Lattice FORTRAN Program for Estimating Subsonic Aerodynamic Characteristics of Complex Planforms. NASA TN D-6142, 1971.
32. Polhamus, Edward C.: A Concept of the Vortex Lift of Sharp-Edge Delta Wings Based on a Leading-Edge-Suction Analogy. NASA TN D-3767, 1966.

1. Report No. NASA RP-1042	2. Government Accession No.	3. Recipient's Catalog No.	
4. Title and Subtitle PERFORMANCE EVALUATION METHOD FOR DISSIMILAR AIRCRAFT DESIGNS		5. Report Date SEPTEMBER 1979	
		6. Performing Organization Code	
7. Author(s) Harold J. Walker		8. Performing Organization Report No. H-1064	
		10. Work Unit No. 505-11-24	
9. Performing Organization Name and Address NASA Dryden Flight Research Center P.O. Box 273 Edwards, California 93523		11. Contract or Grant No.	
		13. Type of Report and Period Covered Reference Publication	
12. Sponsoring Agency Name and Address National Aeronautics and Space Administration Washington, D.C. 20546		14. Sponsoring Agency Code	
		15. Supplementary Notes	
16. Abstract			
<p>A rationale is presented for using the square of the wingspan rather than the wing reference area as a basis for nondimensional comparisons of the aerodynamic and performance characteristics of aircraft that differ substantially in planform and loading. Working relationships are developed and illustrated through application to several categories of aircraft covering a range of Mach numbers from 0.60 to 2.00. For each application, direct comparisons of drag polars, lift-to-drag ratios, and maneuverability are shown for both nondimensional systems. The inaccuracies that may arise in the determination of aerodynamic efficiency based on reference area are noted. Span loading is introduced independently in comparing the combined effects of loading and aerodynamic efficiency on overall performance.</p> <p>Performance comparisons are made for the NACA research aircraft, lifting bodies, century-series fighter aircraft, F-111A aircraft with conventional and supercritical wings, and a group of supersonic aircraft including the B-58 and XB-70 bomber aircraft. An idealized configuration is included in each category to serve as a standard for comparing overall efficiency.</p>			
17. Key Words (Suggested by Author(s)) Performance evaluation method Research aircraft		18. Distribution Statement Unclassified-Unlimited STAR category: 01	
19. Security Classif. (of this report) Unclassified	20. Security Classif. (of this page) Unclassified	21. No. of Pages 73	22. Price* \$4.25

*For sale by the National Technical Information Service, Springfield, Virginia 22161